

Position Sensorless Control of 4S3P Inverter Fed PMSM Drive Based on Artificial Neural Network

by



Kalyan Kumar Halder



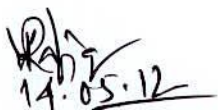
A thesis submitted in partial fulfillment of the requirements for the degree of
Master of Science
in Electrical and Electronic Engineering



Khulna University of Engineering & Technology
Khulna 9203, Bangladesh
May 2012

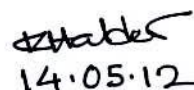
DECLARATION

This is to certify that the thesis work entitled "*Position Sensorless Control of 4S3P Inverter Fed PMSM Drive Based on Artificial Neural Network*" has been carried out by *Kalyan Kumar Halder* in the Department of *Electrical and Electronic Engineering*, Khulna University of Engineering & Technology, Khulna, Bangladesh. The above thesis work or any part of this work has not been submitted anywhere for the award of any degree or diploma.



14.05.12

Signature of Supervisor



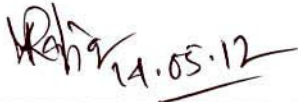
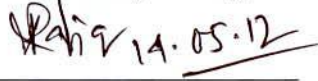

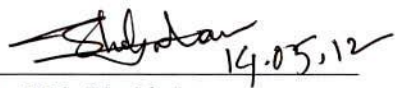
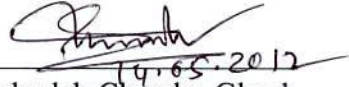
14.05.12

Signature of Candidate

APPROVAL

This is to certify that the thesis work submitted by *Kalyan Kumar Halder* entitled “*Position Sensorless Control of 4S3P Inverter Fed PMSM Drive Based on Artificial Neural Network*” has been approved by the board of examiners for the partial fulfillment of the requirements for the degree of *Master of Science* in the Department of *Electrical and Electronic Engineering*, Khulna University of Engineering & Technology, Khulna, Bangladesh in May 2012.

BOARD OF EXAMINERS

1. 
_____ 14.05.12
Dr. Md. Abdur Rafiq
Professor, Dept. of Electrical and Electronic Engineering
Khulna University of Engineering & Technology
Chairman
(Supervisor)
2. 
_____ 14.05.12
Dr. Md. Abdur Rafiq
Head, Dept. of Electrical and Electronic Engineering
Khulna University of Engineering & Technology
Member
3. 
_____ 14.5.12
Dr. M. A. Samad
Professor, Dept. of Electrical and Electronic Engineering
Khulna University of Engineering & Technology
Member
4. 
_____ 14.05.12
Dr. Md. Shahjahan
Assoc. Professor, Dept. of Electrical and Electronic Engineering
Khulna University of Engineering & Technology
Member
5. 
_____ 14.05.2012
Dr. Bashudeb Chandra Ghosh
Professor, Dept. of Electrical and Electronic Engineering
American International University-Bangladesh
Member
(External)

ACKNOWLEDGEMENT

I wish to express my deep gratitude to my supervisor, Prof. Dr. Md. Abdur Rafiq for his guidance, encouragement, and support during my research work. His creative thinking, knowledge and expertise on electric machines and controls were the “power supply” and “feedback” of my conducted researches.

My appreciation also extends to Prof. Dr. Bashudeb Chandra Ghosh, who brought me into the fantastic world of power electronics and drives, and has always inspired me to strive me the highest level of professionalism. I learned that a qualified researcher should keep open mind and pay persistent effort from him. Without Prof. Ghosh’s guidance and help, any success in my research career will never be possible.

I also acknowledge with gratitude the help of faculty members who have always been willing to discuss and exchange ideas.

I am thankful to the staff members of different laboratories and office of the head of the department.

Last but not the least, I am always indebted to all my family members for their endless support and love. I greatly appreciate the sacrifices they have made over the years, without which the completion of my study would not be possible.

ABSTRACT

A position sensorless Permanent Magnet Synchronous Motor (PMSM) drive based on single layer Recurrent Neural Network (RNN) is presented in this research work. In the proposed control methodology, instead of a usual 6-Switch 3-Phase (6S3P) inverter a 4-Switch 3-Phase (4S3P) inverter is used. This reduces the cost of the inverter, the switching losses, and the complexity of the control board for generating six Pulse Width Modulated (PWM) signals. A simulation model of the drive system is developed and used in this study. The motor equations are written in rotor fixed $d-q$ reference frame. A Proportional plus Integral (PI) controller is used to process the speed error to generate the reference torque current. The RNN estimator is used to estimate stator flux components along the stator fixed stationary axes ($\alpha-\beta$). In this study, the Correlated Real Time Recurrent Learning (CRTRL) algorithm is used for training the neural network. The rotor angle is used in vector rotator to generate the reference phase currents. Hysteresis current controller block controls the switching of the three phase inverter to apply voltage to the motor stator. Numerical simulation is carried out in order to verify the effectiveness of the proposed control system. Simulation studies show that the proposed RNN estimator can be used to accurately measure the motor fluxes and rotor angle over a wide speed range. The robustness of the drive system is tested for different operating conditions, i.e., sudden load torque change, parameter deviation, speed reversal, ramp change of speed, load disturbance, presence of computational error, etc. The control system is found to work acceptably under these conditions. It is also simple and low cost to implement in a practical environment.

Dedicated
To
My Family...

CONTENTS

	PAGE
Title Page	i
Declaration	ii
Approval	iii
Acknowledgement	iv
Abstract	v
Contents	vii
List of Tables	ix
List of Figures	x
Nomenclature	xiii
CHAPTER I	Introduction
1.1	Background of the Study 1
1.2	Objectives of the Study 3
1.3	Dissertation Organization 4
CHAPTER II	Fundamentals of Permanent Magnet Synchronous Motor
2.1	Introduction 6
2.2	Permanent Magnet Materials 6
2.3	Classification of Permanent Magnet Motors 7
2.3.1	Direction of Field Flux 7
2.3.2	Flux Density Distribution 7
2.3.3	Permanent Magnet Radial Field Motors 7
2.4	Comparative Study of AC Drives 9
2.5	Conclusion 14
CHAPTER III	Modeling of the Drive System
3.1	Introduction 15
3.2	Mathematical Model of PMSM 15
3.3	Mathematical Model of 4S3P Inverter 28
3.4	Controller Models 31
3.4.1	PI Controller 31
3.4.2	Hysteresis Current Controller 32
3.5	Conclusion 33
CHAPTER IV	Artificial Neural Network and Proposed Control System
4.1	Introduction 34
4.2	Artificial Neural Network 34
4.2.1	Models of a Neuron 35

4.2.2	Real Time Recurrent Learning Algorithm	38
4.2.3	Proposed Stator Flux Estimation Methodology	40
4.3	Proposed PMSM Control Scheme	43
4.3.1	Adjusting the PI Gains	44
4.3.2	Flux Program	45
4.3.3	Coordinate Transforms	45
4.3.3.1	Vector Rotator	45
4.3.3.2	Clarke Transform	46
4.3.4	Hysteresis Current Control Technique	46
4.4	Conclusion	47
CHAPTER V	Simulation Results and Discussions	
5.1	Introduction	48
5.2	RNN based Stator Flux and Rotor Position Estimation	48
5.3	Starting Performance of the PMSM Drive	51
5.4	Performance under Different Operating Conditions	53
5.4.1	Sudden Change of Load Torque	53
5.4.2	Variation of Stator Parameters	54
5.4.3	Speed Reversal	55
5.4.4	Ramp Speed Change	56
5.4.5	Sudden Disturbance Torque	57
5.4.6	Presence of Computational Errors	58
5.5	Conclusion	59
CHAPTER VI	Conclusions and Suggestions for Future Works	
6.1	Conclusions	60
6.2	Suggestions for Future Works	61
References		62
Appendix		66

LIST OF TABLES

Table No	Description	Page
3.1	Inverter Modes of Operation	30
A1	PMSM Parameters	66

LIST OF FIGURES

Figure No.	Description	Page
2.1	Surface permanent magnet motor.	8
2.2	Interior permanent magnet motor.	9
3.1	Two-pole three phase surface mounted PMSM.	17
3.2	q -axis leading d -axis and the rotor angle represented as θ_r .	20
3.3	q -axis leading d -axis and the rotor angle represented as θ .	22
3.4	PMSM fed from a four switch inverter.	29
3.5	Switching vectors for a four switch inverter.	30
3.6	Waveforms for 3-phase voltages	30
3.7	Block diagram of a PI controller.	32
3.8	Hysteresis controller.	33
4.1	Nonlinear model of a neuron.	36
4.2	Affine transformations produced by the presence of a bias; where $v_k = b_k$ at $u_k = 0$.	36
4.3	Another nonlinear model of a neuron.	37
4.4	Fully connected real time recurrent network.	38
4.5	Block diagram of neural network filter.	41
4.6	Neural filter based integrator.	42
4.7	Stationary α - and β -axis stator flux estimation by CRTRL algorithm.	43
4.8	Proposed control scheme of the PMSM.	44
4.9	Stationary and rotating axes of PMSM.	46
4.10	Hysteresis current controller block diagram.	47
5.1.1	Actual and estimated responses of (a) α -axis stator flux, (b) β - axis stator flux, and (c) Rotor angle for the 4S3P inverter fed PMSM drive (runs at 1500 rpm) under transient condition.	49
5.1.2	Actual and estimated responses of (a) α -axis stator flux, (b) β - axis stator flux, and (c) Rotor angle for the 4S3P inverter fed PMSM drive (runs at 1500 rpm) under steady-state condition.	49

5.1.3	Actual and estimated responses of (a) α -axis stator flux, (b) β -axis stator flux, and (c) Rotor angle for the 4S3P inverter fed PMSM drive (runs at 150 rpm) under transient and steady-state conditions.	49
5.2.1	Actual and estimated responses of (a) α -axis stator flux, (b) β -axis stator flux, and (c) Rotor angle for the 6S3P inverter fed PMSM drive (runs at 1500 rpm) under transient condition.	50
5.2.2	Actual and estimated responses of (a) α -axis stator flux, (b) β -axis stator flux, and (c) Rotor angle for the 6S3P inverter fed PMSM drive (runs at 1500 rpm) under steady-state condition.	50
5.2.3	Actual and estimated responses of (a) α -axis stator flux, (b) β -axis stator flux, and (c) Rotor angle for the 6S3P inverter fed PMSM drive (runs at 150 rpm) under transient and steady-state conditions.	50
5.3	Stator phase voltages for the 4S3P inverter fed PMSM: (a) V_a , (b) V_b , (c) V_c .	51
5.4	Stator phase voltages for the 6S3P inverter fed PMSM: (a) V_a , (b) V_b , (c) V_c .	51
5.5	(a) Speed, (b) Developed electromagnetic torque, (c) command currents, and (d) actual motor currents for the 4S3P inverter fed PMSM drive.	52
5.6	(a) Speed, (b) Developed electromagnetic torque, (c) command currents, and (d) actual motor currents for the 6S3P inverter fed PMSM drive.	53
5.7	(a) Estimated rotor angle, (b) Speed, (c) Developed electromagnetic torque, and (d) Three phase currents for the proposed PMSM drive for change of load torque.	54
5.8	a) Estimated rotor angle, (b) Speed, (c) Developed electromagnetic torque, and (d) Three phase currents for the proposed PMSM drive for change of stator resistance.	55
5.9	a) Estimated rotor angle, (b) Speed, (c) Developed electromagnetic torque, and (d) Three phase currents for the proposed PMSM drive under speed reversal.	56

5.10	a) Estimated rotor angle, (b) Speed, (c) Developed electromagnetic torque, and (d) Three phase currents for the proposed PMSM drive under ramp speed change.	57
5.11	a) Estimated rotor angle, (b) Speed, (c) Developed electromagnetic torque, and (d) Three phase currents for the proposed PMSM drive for sudden disturbance torque.	58
5.12	a) Estimated rotor angle, (b) Speed, (c) Developed electromagnetic torque, and (d) Three phase currents for the proposed PMSM drive for computational error.	59

NOMENCLATURE

$\vec{v}_s, \vec{i}_s, \vec{\lambda}_s$	complex space vectors of the three phase stator voltages, currents, and flux linkages
v_{sa}, v_{sb}, v_{sc}	three phase stator instantaneous phase voltages
i_{sa}, i_{sb}, i_{sc}	three phase stator instantaneous phase currents
$\lambda_{sa}, \lambda_{sb}, \lambda_{sc}$	three phase stator flux linkages
r_a, r_b, r_c	three phase stator resistances
L_{aa}, L_{bb}, L_{cc}	self-inductances of the stator <i>a-b-c</i> - phases
L_{ab}, L_{bc}, L_{ac}	mutual inductances between the <i>a-b-c</i> phases
$\lambda_{ra}, \lambda_{rb}, \lambda_{rc}$	flux linkages in stator <i>a-b-c</i> - windings changing with rotor angle
r_s	resistance of the stator winding
λ_r	peak flux linkage due to the permanent magnet
k_e	back-EMF constant
L_{ls}	leakage inductance of stator winding due to armature leakage flux
L_{ms}	inductance fluctuation due to the rotor position dependent on flux
L_0	average inductance due to the space fundamental air-gap flux
L_{ss}	stator inductance matrix
θ_r	rotor angle
λ_d, λ_q	<i>d</i> -and <i>q</i> -axis stator flux linkages
L_d, L_q	<i>d</i> -and <i>q</i> -axis stator synchronous inductances
L_{mq}, L_{md}	common mutual inductances on the <i>d</i> -axis and <i>q</i> -axis circuits
p	derivative of time
ω_r	angular velocity
α, β	orthogonal axes of stationary reference frame
$d - q$	synchronously rotating reference frame
a, a^2	spatial operators for orientation of the stator windings
P_p	number of pole pairs



P_i	instantaneous input power
v_d, v_q	d -and q -axis stator voltage components
i_d, i_q	d -and q -axis stator current components
ω_m	angular speed of the motor
T_L	load torque
B_m	rotational damping coefficient
J_m	moment of inertia
$[v_s]$	Three phase applied voltages in matrix form
$[i_s]$	three phase stator currents in matrix form
$[\Lambda_s]$	three-phase stator flux linkages in matrix form
$i_{\alpha s}, i_{\beta s}$	α -and β -axis stator current components
$\lambda_{\alpha s}, \lambda_{\beta s}$	α -and β -axis stator flux linkages
E_ω	speed error
i_a^*, i_b^*, i_c^*	three phase stator reference currents
i_m^*, i_t^*	magnetizing and torque producing stator current components
ω_{ref}	motor command speed
K_p, K_i	PI gains
b_k	bias of the neuron k
x_m	input signal of the neuron k
w_{km}	synaptic weight of the neuron k to m
u_k	linear combiner output due to the input signals
$\phi(\cdot)$	activation function
y_k	output signal of the neuron k
$x(n)$	signal vector at the time step n
$\xi(n)$	cost function at the time step n
$\Lambda_j(n)$	partial derivative matrix of the state vector $x(n)$ with respect to the weight vector w_j
$U_j(n)$	q -by- $(q + m + 1)$ matrix whose rows are all zero,

$\phi(n)$	q -by- q diagonal matrix whose k th diagonal element is the partial derivative of the activation function with respect to its argument
$\xi(n)$	the $(q+m+1)$ -by-1 vector
ΔW_j	adjustment for the weight vector of the j th neuron
$\tilde{y}(n)$	desired output vector
Z^{-1}	unit-delay operator
G	gain function
T_s	sampling time
η	rate of learning
τ	time constant

CHAPTER I

Introduction

1.1 Background of the Study

Dc motor drives dominated the fields of variable speed drives from the 19th century to the last decades of the 20th century. The controllability of dc drives was superior to those of ac drives. At the end of the 1960s K. Hasse introduced the Field Oriented Control (FOC) of ac motor. It was pointed out that in theory the Induction Motor (IM) can be controlled in the same way as the dc motor. The development of semiconductor power devices made it possible to build frequency converters for ac motors allowing a sinusoidal three phase current supply with continuous frequency control. In the 1980s frequency converter fed ac drives using FOC became competitive with dc drives commercially. Since then the percentual share of dc drives has declined because the ac motor has several benefits compared to the dc motor. They are inexpensive, and have low maintenance compared with dc motors. The speed range of ac motor is wider and the machine size is smaller in the same power class [1]. All kinds of electrical ac drives have been developed and applied, which serve to drive manufacturing facilities such as conveyor belts, robot arms, cranes, steel process lines, paper mills, waste water treatment and so on.

Among the ac drives, Permanent Magnet Synchronous Motor (PMSM) drives have been increasingly applied in a wide variety of industrial applications [2]. These motors have been used in several areas such as traction, automobiles, robotics, and aerospace technology [3]. The power density of PMSM is higher than that of IM with the same ratings because no stator power is required for the magnetic field production. Now a days, PMSMs are designed not only to be more powerful but also with lower mass and lower moment of inertia [4]. The continuous cost reduction of magnetic materials with high energy density and coercitivity (e.g., samarium cobalt and neodymium-boron iron) makes the ac drives based on PMSM more attractive and competitive. In the high performance applications, the PMSM drives are ready to meet sophisticated requirements such as fast dynamic response, high power factor and wide operating speed range. This has opened up

new possibilities for large-scale application of PMSM. Consequently, a continuous increase in the use of PMSM drives will surely be witnessed in the near future [5-7].

With the invention of high speed power semiconductor devices 6-Switch 3-Phase (6S3P) inverters become popular for variable speed ac drives. These inverters have some disadvantages such as losses in the six switches, complexity of the control algorithms and generating six PWM logic signals [8-12]. Many researchers have been working in this area to reduce the inverter size and cost without altering the drive performances. In [8], an ac to ac converter was developed for IM with least hardware and improved power factor. A cost effective 4-Switch 3-Phase (4S3P) inverter was proposed for IM and PMSM drives in [9-10]. The inverter consists of four switches instead of six and hence improves the inverter performance. The authors also showed a performance comparison of the 4S3P inverter fed drive with 6S3P inverter fed drive in terms of speed response and total harmonic distortion of the stator current. A Fuzzy Logic based control scheme was proposed for 4S3P fed PMSM drive in [11]. A vector control scheme of IM using 4S3P inverter for high performance industrial drive systems was presented in [12]. The complete vector control scheme was verified by simulation and experimentation in a DSP environment. Therefore, 4S3P inverter is becoming better candidate of power inverters.

Driving a PMSM requires the rotor position information to control the motor torque which is generally detected by mechanical position sensors such as an encoder or a resolver. In cost sensitive applications like appliance drives or in a hostile environment, a mechanical shaft encoder can often not be used. However, position sensors make the total system larger in volume, and less reliable. In [13] a mathematical model of PMSM using the extended electromotive force in the rotating reference frame was utilized to estimate the rotor speed and position. A completely encoder-less PMSM drive with direct torque controller was proposed in [14]. The authors used a new sliding mode observer for speed estimation. Interior Permanent Magnet (IPM) motors possess magnetic saliency that introduces harmonic in the motor current. This phenomenon can be utilized to find out the rotor speed and position of the interior IPM drives [15]. In [16] the authors presented a novel class of V/f sensorless AC general drives with two stabilizing loops-one based on active flux balance and one based on speed error that provide fast speed dynamics response

without steady state error and without speed or current regulators. Sensorless control scheme for PMSM drives based on high-frequency carrier injection was proposed in [17].

In Recent years, Artificial Neural Network (ANN) has been used in AC drive systems because of their adaptive, learning and observing function talents. A stator-flux-oriented vector controlled IM drive was proposed in [18] where the space vector pulse width modulation and stator flux estimation were implemented by ANNs. A robust adaptive speed sensorless IM drive using an ANN was presented in [19]. The authors proposed a speed controller using the neural network uncertainty observer. A neural network based rotor position control and speed estimation method for PMSM was proposed in [20]. The proposed method had three recurrent neural networks which were used for estimating stator current, rotor speed, and rotor position angle. In [21], the authors proposed a simple neural network based rotor flux estimator for high performance IM drives. Their proposed method was claimed to be accurate for measurement of the rotor flux including its magnitude and phase angle at various conditions like sudden speed change and load torque disturbance. In [22], a Total Least Squares (TLS) algorithm based speed and position estimation algorithm for PMSM drives was used. This algorithm utilized the stator voltages and currents measured from the PMSM drive to obtain the estimated speed. A fuzzy neural network suitable for practical implementation was proposed in [23]. A sensorless control strategy for PMSM control using a novel neural network algorithm was presented in [24]. The proposed observer used a neural network trained to learn the electrical and mechanical motor models using the current prediction error.

There are several algorithms for learning neural network like Back Propagation (BP) algorithm, Uncorrelated Real Time Recurrent Learning (URTRL) algorithm and Correlated Real Time Recurrent Learning (CRTRL) algorithm. Among them CRTRL algorithm based methodology provides better performance than the other two algorithms [25].

1.2 Objectives of the Study

Most of the previous researches on PMSM drives were carried out either to remove the position and speed sensors or to reduce the three phase inverter size for cost effective and reliable operation. There is no study on PMSM drives which considers both the 4S3P

inverter and ANN based position sensorless control scheme. This research is expected to contribute new realistic technique to the design of position sensorless vector control of PMSM drive with 4S3P inverter. On this purpose, a simulation model of the PMSM drive system has been deduced. The main objectives of this research work include:

- Propose a 4S3P inverter instead of conventional 6S3P inverter for the PMSM drives.
- Propose an ANN based adaptive integration methodology for estimating the rotor position angle of PMSM that is able to work over wide speed range.
- Develop a CRTRL algorithm for training the proposed neural network.
- Develop a vector control scheme that can be easily implemented in a low-cost DSP-based digital controller.
- Investigate the control scheme in terms of competence and robustness of operation at different operating conditions.

1.3 Dissertation Organization

The total research work has been divided into several components and presented literally in six chapters including introduction and conclusion. The dissertation is organized as follows:

Chapter I introduces the background for this dissertation research, the significance of the study and the research objectives.

Chapter II reviews the state of the art and recent developments of magnetic materials, and permanent magnet synchronous motors. A classification of the permanent magnet motors is also given. It also includes a comparative study between permanent magnet motors and other ac motors.

Chapter III deals with the mathematical modeling. It provides a detailed analysis of the mathematical model of permanent magnet synchronous motor. This is followed by the modeling of 4-switch 3-phase inverter, PI controller and hysteresis current controller.

Chapter IV presents the proposed position sensorless control scheme of PMSM. Preliminary ideas of artificial neural network and correlated real time recurrent learning

algorithm for the recurrent neural network are discussed here. Neural network based stator flux and rotor position estimation technique is also presented in this chapter. Finally, it provides brief descriptions of different components of the proposed control scheme.

Chapter V is dedicated to computer simulation. Simulation model of the permanent magnet synchronous motor is deduced and results of simulation for different operating conditions are shown. At the first stage, the performance of the flux and position estimator is investigated. Then the starting performances of the motor are illustrated under transient and steady-state conditions. Finally, robustness of the control scheme is examined to load fluctuations, speed variation, and parameter perturbation, etc.

Chapter VI gives the overall conclusions of the research with a few proposals for further research work.



CHAPTER II

Fundamentals of Permanent Magnet Synchronous Motor

2.1 Introduction

The Permanent magnet motor is a motor that uses permanent magnets to produce the air gap magnetic field rather than using electromagnets. These motors have significant advantages, attracting the interest of the researchers and industry for use in many applications. This chapter deals with the description of the different components of permanent magnet synchronous motors before proceeding to design control algorithms for them. Initially, a review of permanent magnet materials and classification of permanent magnet motors is given. Finally a comparison of permanent magnet motors over other ac motors is presented in brief.

2.2 Permanent Magnet Materials

The properties of the permanent magnet material will affect directly the performance of the motors and proper knowledge is required for the selection of the materials and for understanding PM motors. The earliest manufactured magnet materials were hardened steel. Magnets made from steel were easily magnetized. However, they could hold very low energy and it was easy to demagnetize. In recent years other magnet materials such as Aluminum Nickel and Cobalt alloys (ALNICO), Strontium Ferrite or Barium Ferrite (Ferrite), Samarium Cobalt (First generation rare earth magnet) (SmCo) and Neodymium Iron-Boron (Second generation rare earth magnet) (NdFeB) have been developed and used for making permanent magnets. The rare earth magnets are categorized into two classes: Samarium Cobalt (SmCo) magnets and Neodymium Iron Boride (NdFeB) magnets. SmCo magnets have higher flux density levels but they are very expensive. NdFeB magnets are the most common rare earth magnets used in motors these days.

2.3 Classification of Permanent Magnet Motors

2.3.1 Direction of Field Flux

PM motors are broadly classified by the direction of the field flux. The first field flux classification is radial field motor meaning that the flux is along the radius of the motor. The second is axial field motor meaning that the flux is perpendicular to the radius of the motor. Radial field flux is most commonly used in motors and axial field flux have become a topic of interest for study and used in a few applications.

2.3.2 Flux Density Distribution

PM motors are classified on the basis of the flux density distribution and the shape of current excitation. They are PMSM and PM brushless motors (BLDC). The PMSM has a sinusoidal-shaped back EMF and is designed to develop sinusoidal back EMF waveforms. They have the following:

1. Sinusoidal distribution of magnet flux in the air gap
2. Sinusoidal current waveforms
3. Sinusoidal distribution of stator conductors.

BLDC has a trapezoidal-shaped back EMF and is designed to develop trapezoidal back EMF waveforms. They have the following:

1. Rectangular distribution of magnet flux in the air gap
2. Rectangular current waveform
3. Concentrated stator windings

2.3.3 Permanent Magnet Radial Field Motors

In PM motors, the magnets can be placed in two different ways on the rotor. Depending on the placement they are called either as surface permanent magnet motor or interior permanent magnet motor.

Surface mounted PM motors have a surface mounted permanent magnet rotor. Each of the PM is mounted on the surface of the rotor, making it easy to build, and specially skewed poles are easily magnetized on this surface mounted type to minimize cogging torque. This

configuration is used for low speed applications because of the limitation that the magnets will fly apart during high-speed operations. These motors are considered to have small saliency, thus having practically equal inductances in both axes. The permeability of the permanent magnet is almost that of the air, thus the magnetic material becoming an extension of the air gap. For a surface permanent magnet motor $L_d = L_q$.

The rotor has an iron core that may be solid or may be made of punched laminations for simplicity in manufacturing. Thin permanent magnets are mounted on the surface of this core using adhesives. Alternating magnets of the opposite magnetization direction produce radially directed flux density across the air gap. This flux density then reacts with currents in windings placed in slots on the inner surface of the stator to produce torque. Fig. 2.1 shows the placement of the magnet.

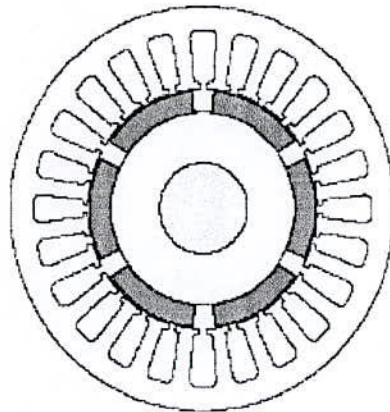


Figure 2.1 Surface permanent magnet motor.

Interior PM motors have interior mounted permanent magnet rotor as shown in Fig. 2.2. Each permanent magnet is mounted inside the rotor. It is not as common as the surface mounted type but it is a good candidate for high-speed operation. There is inductance variation for this type of rotor because the permanent magnet part is equivalent to air in the magnetic circuit calculation. These motors are considered to have saliency with q -axis inductance greater than the d -axis inductance ($L_q > L_d$).

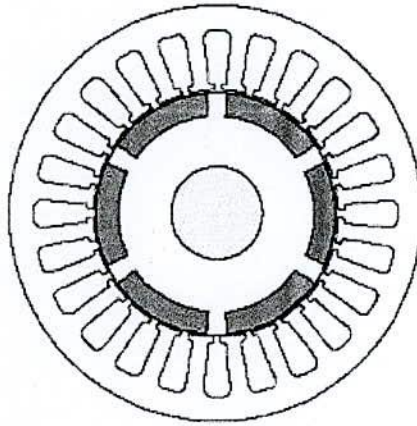


Figure 2.2 Interior permanent magnet motor.

2.4 Comparative Study of AC Drives

Recent availability of high energy-density PM materials at competitive prices, continuing breakthroughs and reduction in cost of powerful fast Digital Signal Processors (DSPs) and micro-controllers combined with the remarkable advances in semiconductor switches and modern control technologies have opened up new possibilities for permanent magnet motor drives in order to meet competitive worldwide market demands [26].

The popularity of PMSMs comes from their desirable features [27]:

- High efficiency
- High torque to inertia ratio
- High torque to volume ratio
- High air gap flux density
- High power factor
- High acceleration and deceleration rates
- Lower maintenance cost
- Simplicity and ruggedness
- Compact structure
- Linear response in the effective input voltage

However, the higher initial cost, operating temperature limitations, and danger of demagnetization mainly due to the presence of permanent magnets can be restrictive for some applications.

In PMSMs, permanent magnets are mounted inside or outside of the rotor. Unlike DC brush motors, every brushless DC (so called BLDC) and permanent magnet synchronous motor requires a “drive” to supply commutated current. This is obtained by pulse width modulation of the DC bus using a DC-to-AC inverter attached to the motor windings. The windings must be synchronized with the rotor position by using position sensors or through sensorless position estimation techniques. By energizing specific windings in the stator, based on the position of the rotor, a rotating magnetic field is generated. In permanent magnet ac motors with sinusoidal current excitation (so called PMSM), all the phases of the stator windings carry current at any instant, but in permanent magnet AC motors with quasi-square wave current excitation (BLDC), only two of the three stator windings are energized in each commutation sequence [26].

In both motors, currents are switched in a predetermined sequence and hence the permanent magnets that provide a constant magnetic field on the rotor follow the rotating stator magnetic field at a constant speed. This speed is dependent on the applied frequency and pole number of the motor. Since the switching frequency is derived from the rotor, the motor cannot lose its synchronism. The current is always switched before the permanent magnets catch up; therefore the speed of the motor is directly proportional to the current switching rate [28].

Like DC brush motors, torque control in AC motors is achieved by controlling the motor currents. However, unlike DC brush motor, in AC motors both the phase angle and the modulus of the current has to be controlled, in other words the current vector should be controlled. That is why the term “vector control” is used for AC motors. In DC brush motors the field flux and armature MMF are coupled, whereas in AC motors the rotor flux and the spatial angle of the armature MMF require external control. Without this type of control, the spatial angle between various fields in the AC motor will vary with the load and cause unwanted oscillating dynamic response. With vector control of AC motors, the torque and flux producing current components are decoupled resembling a DC brush

motor, the transient response characteristics are similar to those of a separately excited DC motor, and the system will adapt to any load disturbances and/or reference value variations as fast as a brushed-DC motor [27].

The main advantages of using permanent magnets over field excitation circuit used by conventional synchronous motors are given below [27]:

- Elimination of slip-rings and extra DC voltage supply.
- No rotor copper losses generated in the field windings of wound-field synchronous motor.
- Higher efficiency because of lesser losses.
- Since there is no circuit creating heat on the rotor, cooling of the motor just through the stator in which the copper and iron losses are observed is more easily achieved.
- Reduction of machine size because of high efficiency.
- Different size and different arrangements of permanent magnets on the rotor will lead to have wide variety of machine characteristics.

PMAC motors have gained more popularity especially after the advent of high performance rare-earth permanent magnets, like samarium cobalt and neodymium-boron iron which surpass the conventional magnetic material in DC brush and are becoming more and more attractive for industrial applications.

The positive specific characteristics of PMAC motors explained above make them highly attractive candidates for several classes of drive applications, such as in servo-drives containing motors with a low to mid power range, robotic applications, motion control system, aerospace actuators, low integral-hp industrial drives, fiber spinning and so on. Also high power rating PMAC motors have been built, for example, for ship propulsion drives up to 1 MW. Recently two major sectors of consumer market are starting to pay more attention to the PM motor drive due to its features.

PMAC motors have many advantages over DC brush motors and IMs. Most of these are summarized as [26]:

- High dynamic response
- High efficiency providing reduction in machine size
- Long operating life
- Noiseless operation
- High power factor
- High power to weight ratio; considered the best comparing to other available electric motors
- High torque to inertia ratio; providing quick acceleration and deceleration for short time
- High torque to volume ratio
- High air-gap flux density
- Higher speed ranges
- Better speed versus torque characteristics
- Lower maintenance cost
- Simplicity and ruggedness
- Compact design
- Linear response
- Controlled torque at zero speed

Compared to IMs, PMSMs have some advantages, such as higher efficiency in steady-state, and operate constantly at synchronous speed. They do not have losses due to the slip which occurs when the rotor rotates at a slightly slower speed than the stator because the process of electromagnetic induction requires relative motion called “slip” between the rotor conductors and the stator rotating field that is special to IM operation. The slip makes the IM asynchronous, meaning that the rotor speed is no longer exactly proportional to the supply frequency [26].

In IMs, stator current has both magnetizing and torque-producing components. On the other hand, in PMSMs there is no need to supply magnetizing current through the stator for constant air-gap flux. Since the permanent magnet generates constant flux in the rotor, the stator current is needed for torque component production only. For the same output, the PMSM will operate at a higher power factor and will be more efficient than the IM [26].

Finally, since the magnetizing is provided from the rotor circuit by permanent magnets instead of the stator, the motor can be built with a large air gap without losing performance. According to the above results, the PMSM has a higher efficiency, torque to ampere rating, effective power factor and power density when compared with an IM. Combining these factors, small PM synchronous motors are suitable for certain high performance applications such as robotics and aerospace actuators in which there is a need for high torque/inertia ratio [26].

Induction machine drives have been widely used in industry. Squirrel-cage induction machines have become popular drive motors due to their simple, rugged structure, ease of maintenance, and low cost. In pumps, fans, and general-purpose drive systems, they have been a major choice. In servo applications, PM motor drives are more popular due to their high output torque performance. They are also actively used in high-speed applications, not only as motors/starters but also as generators, as in the Flywheel Energy Storage System (FEES), Electric Vehicle (EV), and Industrial Turbo-Generator (ITG) system.

The smaller the motor size required, the more preferable it is to use permanent magnet synchronous motors. As motor size increases the cost of the magnetics increases as well making large PMACs cost ineffective. There is no actual "breakpoint" under which PMSMs outperform IMs, but the 1-10 kW range is a good estimate of where they do. As compared with induction and conventional wound-rotor synchronous motors (WRSM), PMSMs have certain advantages over both motors, including the fact that there is no field winding on the rotor as compared to the WRSM; therefore there are no attendant copper losses. Moreover, there is no circuit in the rotor but only in the stator where heat can be removed more easily [26].

Compared with conventional WRSMs, elimination of the field coil, DC supply, and slip rings result in a much simpler motor. In a PMSM, there is no field excitation control. The control is provided by just stator excitation control. Field weakening is possible by applying a negative direct axis current in the stator to oppose the rotor magnet flux. Elimination of the need for separate field excitation results in smaller overall size such that

for the same field strength the diameter of a PMSM is considerably smaller than its wound field counterpart, providing substantial savings in both size and weight.

2.5 Conclusion

A detailed discussion on the permanent magnet motor is presented in this chapter. The properties of magnetic materials directly affect the performance of the permanent magnet motors. Therefore, a brief description on the commercially available magnetic materials is presented here. A classification of permanent magnet motors depending on various characteristics is included also. The advantages and disadvantages of permanent magnet motors over induction motors, DC brush motors, etc in various aspects is also presented. The above discussion proves the superiority of the permanent magnet synchronous motor for industry applications.

CHAPTER III

Modeling of the Drive System

3.1 Introduction

The aim of this chapter is to systemically review mathematical models of the two major varieties of permanent-magnet synchronous machines, namely interior PM motors and surface-mounted PM motors, before proceeding to design control and observation algorithms for them. Transformations of variables are used to deal with the time-varying machine inductances, referring to the coefficients of differential equations (e.g., voltage equations) that describe the performance and behavior of the PM motors. Moreover, basic operating principles of different current controllers are discussed. All the analysis presented in the later chapters is based on these models.

3.2 Mathematical Model of PMSM

In a PMSM where the inductances vary as a function of the rotor angle, the two-phase (d - q) equivalent circuit model is a perfect solution to analyze the multiphase machines because of its simplicity and intuition. Conventionally, a two-phase equivalent circuit model instead of complex three-phase model has been used to analyze reluctance synchronous machines [29]. This theory is now applied in the analysis of other types of motors including PMSMs, IMs etc.

In this section, an equivalent two-phase circuit model of a three-phase PMSM (interior and surface mount) is derived in order to clarify the concept of the transformation (Park) and the relation between three-phase quantities and their equivalent two-phase quantities. Throughout the derivation of the two-phase (d - q) mathematical model of PMSM, the following assumptions are made [30]:

- Stator windings produce sinusoidal MMF distribution. Space harmonics in the air-gap are neglected.
- Air-gap reluctance has a constant component as well as a sinusoidal varying component.

- Balanced three-phase sinusoidal supply voltage is considered.
- Eddy current and hysteresis effects are neglected.
- Presence of damper windings is not considered; PMSMs used today rarely have that kind of configuration.

Comparing a primitive version of a PMSM with wound-rotor synchronous motor, the stator of a PMSM has windings similar to those of the conventional wound-rotor synchronous motor which is generally three-phase, Y-connected, and sinusoidally distributed. However, on the rotor side instead of the electrical-circuit seen in the wound-rotor synchronous motor, constant rotor flux (λ_r) provided by the permanent magnet in/on the rotor should be considered in the d - q model of a PMSM.

The space vector form of the stator voltage equation in the stationary reference frame is given as:

$$\vec{v}_s = r_s \vec{i}_s + \frac{d \vec{\lambda}_s}{dt} \quad (3.1)$$

where, r_s , \vec{v}_s , \vec{i}_s , and $\vec{\lambda}_s$ are the resistance of the stator winding, complex space vectors of the three phase stator voltages, currents, and flux linkages, all expressed in the stationary reference frame fixed to the stator, respectively. They are defined as:

$$\begin{aligned} \vec{v}_s &= \frac{2}{3} [v_{sa}(t) + a v_{sb}(t) + a^2 v_{sc}(t)] \\ \vec{i}_s &= \frac{2}{3} [i_{sa}(t) + a i_{sb}(t) + a^2 i_{sc}(t)] \\ \vec{\lambda}_s &= \frac{2}{3} [\lambda_{sa}(t) + a \lambda_{sb}(t) + a^2 \lambda_{sc}(t)] \end{aligned} \quad (3.2)$$

The resultant voltage, current, and flux linkage space vectors shown in (3.2) for the stator are calculated by multiplying instantaneous phase values by the stator winding orientations in which the stator reference axis for the a -phase is chosen to the direction of maximum MMF. Reference axes for the b - and c - stator frames are chosen 120° and 240° (electrical degree) ahead of the a -axis, respectively. Fig. 3.1 illustrates a conceptual cross-sectional view of a three-phase, two-pole surface PM synchronous motor along with the two-phase d - q rotating reference frame.

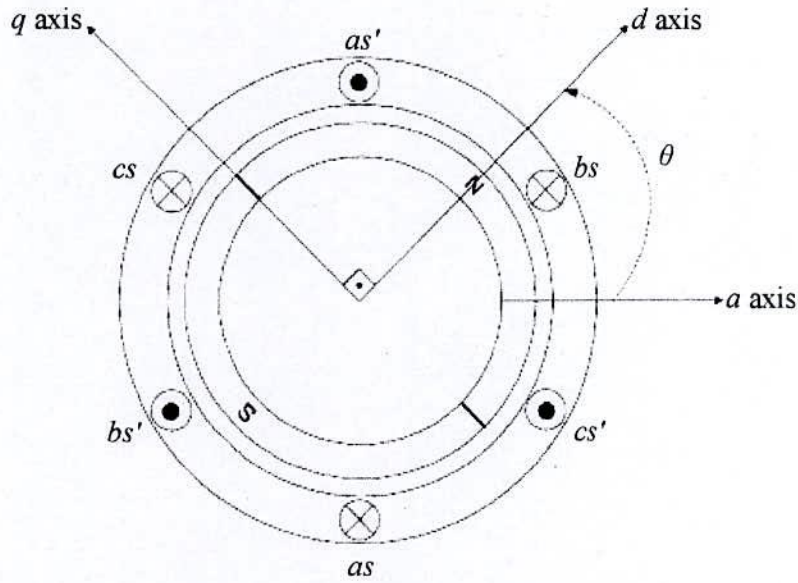


Figure 3.1 Two-pole three phase surface mounted PMSM.

Symbols used in (3.2) are explained in detail below:

a , and a^2 are spatial operators for orientation of the stator windings; $a = e^{j2\pi/3}$,

$$a^2 = e^{j4\pi/3}$$

v_{sa} , v_{sb} , and v_{sc} are the values of stator instantaneous phase voltages.

i_{sa} , i_{sb} , and i_{sc} are the values of stator instantaneous phase currents.

λ_{sa} , λ_{sb} , and λ_{sc} are the stator flux linkages and are given by:

$$\lambda_{sa} = L_{aa}i_a + L_{ab}i_b + L_{ac}i_c + \lambda_{ra}$$

$$\lambda_{sb} = L_{ab}i_a + L_{bb}i_b + L_{bc}i_c + \lambda_{rb}$$

$$\lambda_{sc} = L_{ac}i_a + L_{bc}i_b + L_{cc}i_c + \lambda_{rc}$$

(3.3)

where,

L_{aa} , L_{bb} , and L_{cc} are the self-inductances of the stator a -phase, b -phase, and c -phase respectively.

L_{ab} , L_{bc} , and L_{ac} are the mutual inductances between the a - and b -phases, b - and c -phases, and a - and c -phases, respectively.

λ_{ra} , λ_{rb} , and λ_{rc} are the flux linkages that change depending on the rotor angle established in the stator a -, b -, and c -phase windings, respectively, due to the presence of the permanent magnet on the rotor. They are expressed as:

$$\begin{aligned}\lambda_{ra} &= \lambda_r \cos \theta \\ \lambda_{rb} &= \lambda_r \cos(\theta - 120^\circ) \\ \lambda_{rc} &= \lambda_r \cos(\theta + 120^\circ)\end{aligned}\tag{3.4}$$

In (3.4), λ_r represents the peak flux linkage due to the permanent magnet. It is often referred to as the back-EMF constant, k_e .

It can be seen in Fig. 3.1 that the direction of permanent magnet flux is chosen as the d -axis, while the q -axis is 90° ahead of the d -axis. The symbol, θ , represents the angle of the q -axis with respect to the a -axis.

Note that in the flux linkage equations, inductances are the functions of the rotor angle, θ . Self-inductance of the stator a -phase winding, L_{aa} , including leakage inductance and a - and b -phase mutual inductance, $L_{ab} = L_{ba}$, have the form:

$$\begin{aligned}L_{aa} &= L_{ls} + L_0 - L_{ms} \cos(2\theta) \\ L_{ab} = L_{ba} &= -\frac{1}{2}L_0 - L_{ms} \cos\left(2\theta - \frac{2\pi}{3}\right)\end{aligned}\tag{3.5}$$

where, L_{ls} is the leakage inductance of the stator winding due to the armature leakage flux, L_0 is the average inductance; due to the space fundamental air-gap flux; $L_0 = \frac{1}{2}(L_q + L_d)$, L_{ms} is the inductance fluctuation (saliency); due to the rotor position dependent on flux; $L_{ms} = \frac{1}{2}(L_q - L_d)$.

For mutual inductance, $L_{ab} = L_{ba}$, in the above equation, a $-(1/2)$ coefficient appears due to the fact that stator phases are displaced by 120° , and $\cos(120^\circ) = -1/2$.

Similar to that of L_{aa} , but with θ replaced by $\left(\theta - \frac{2\pi}{3}\right)$ and $\left(\theta - \frac{4\pi}{3}\right)$, b -phase and c -phase self-inductances, L_{bb} and L_{cc} can also be obtained, respectively. Also, a similar

expression for L_{bc} and L_{ac} can be provided by replacing θ in (3.5) with $\left(\theta - \frac{2\pi}{3}\right)$ and $\left(\theta - \frac{4\pi}{3}\right)$, respectively.

All stator inductances are represented in matrix form below:

$$L_{ss} = \begin{bmatrix} L_{ls} + L_0 - L_{ms} \cos 2\theta & -\frac{1}{2}L_0 - L_{ms} \cos 2\left(\theta - \frac{\pi}{3}\right) & -\frac{1}{2}L_0 - L_{ms} \cos 2\left(\theta + \frac{\pi}{3}\right) \\ -\frac{1}{2}L_0 - L_{ms} \cos 2\left(\theta - \frac{\pi}{3}\right) & L_{ls} + L_0 - L_{ms} \cos 2\left(\theta - \frac{2\pi}{3}\right) & -\frac{1}{2}L_0 - L_{ms} \cos 2(\theta - \pi) \\ -\frac{1}{2}L_0 - L_{ms} \cos 2\left(\theta + \frac{\pi}{3}\right) & -\frac{1}{2}L_0 - L_{ms} \cos 2(\theta + \pi) & L_{ls} + L_0 - L_{ms} \cos 2\left(\theta + \frac{2\pi}{3}\right) \end{bmatrix} \quad (3.6)$$

It is evident from (3.6) that the elements of L_{ss} are a function of the rotor angle which varies with time at the rate of the speed of rotation of the rotor.

Under a three-phase balanced system with no rotor damping circuit and knowing the flux linkages, stator currents, and resistances of the motor, the electrical three-phase dynamic equation in terms of phase variables can be arranged in matrix form similar to that of (3.1) written as:

$$[v_s] = [r_s][i_s] + \frac{d}{dt}[\Lambda_s] \quad (3.7)$$

where,

$$\begin{aligned} [v_s] &= [v_{sa} \quad v_{sb} \quad v_{sc}]^t \\ [i_s] &= [i_{sa} \quad i_{sb} \quad i_{sc}]^t \\ [r_s] &= \text{diag}[r_a \quad r_b \quad r_c]^t \\ [\Lambda_s] &= [\lambda_{sa} \quad \lambda_{sb} \quad \lambda_{sc}]^t \end{aligned} \quad (3.8)$$

In (3.7), $[v_s]$, $[i_s]$, and $[\Lambda_s]$ refer to the three-phase applied voltages, three-phase stator currents, and three-phase stator flux linkages in matrix forms as shown in (3.8), respectively. Furthermore, $[r_s]$ is the diagonal matrix in which under balanced three-phase conditions, all phase resistances are equal to each other and represented as a constant, $r_s = r_a = r_b = r_c$, not in matrix form.

The matrix representation of the flux linkages of the three-phase stator windings can also be expressed with using equations (3.3), (3.6) and (3.8) as

$$[\Lambda_s] = L_{ss}[i_s] + [\Lambda_r] \quad (3.9)$$

where, L_{ss} is the stator inductance matrix varying with rotor angle. $[\Lambda_r]$ is the flux linkage matrix due to permanent magnet; $[\Lambda_r] = [\lambda_{ra} \quad \lambda_{rb} \quad \lambda_{rc}]^t$.

As it was discussed before, L_{ss} has time-dependent coefficients which present computational difficulty when (3.1) is being used to solve for the phase quantities directly. To obtain the phase currents from the flux linkages, the inverse of the time-varying inductance matrix will have to be computed at every time step. The computation of the inverse at every time step is time-consuming and could produce numerical stability problems.

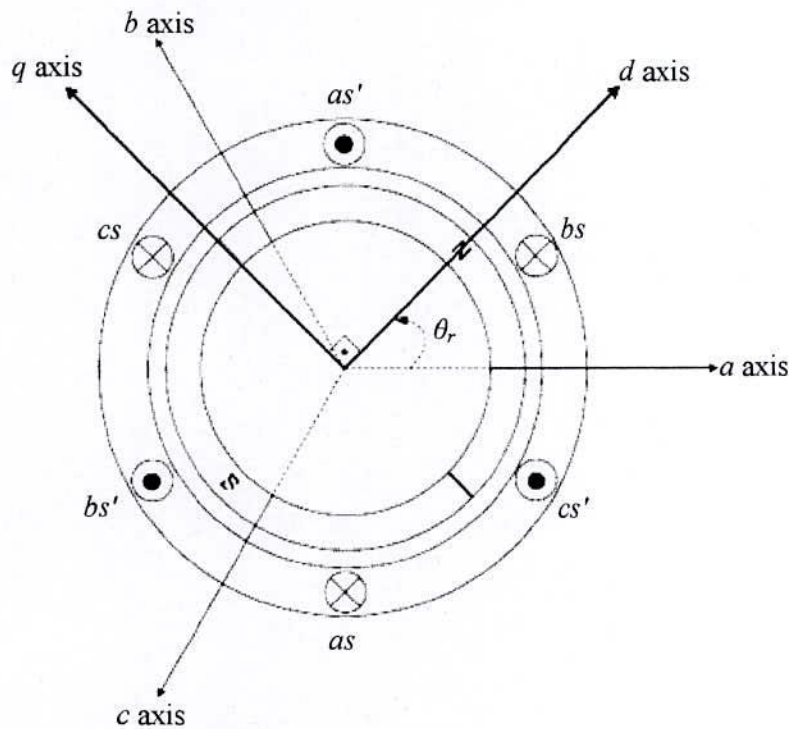


Figure 3.2 q -axis leading d -axis and the rotor angle represented as θ_r .

To remove the time-varying quantities in voltages, currents, flux linkages and phase inductances, stator quantities are transformed to a d - q rotating reference frame. This results in the voltages, currents, flux linkages, part of the flux linkages equation and inductance equations having time-invariant coefficients. In the idealized machine, the rotor windings are already along the q - and d -axis, only the stator winding quantities need transformation from three-phase quantities to the two-phase d - q rotor rotating reference frame quantities. To do so, Park's Transformation is used to transform the stator quantities of an AC machine onto a d - q reference frame that is fixed to the rotor, with the positive d -axis

aligned with the magnetic axis of the rotor which has a permanent magnet in PMSMs. The positive q -axis is defined as leading the positive d -axis by $\pi/2$ in the original Park's Transformation, as shown in Fig. 3.2. The original Park's Transformation equation is of the form:

$$[f_{dq0}] = [T_{dq0}(\theta_r)][f_{abc}] \quad (3.10)$$

where the d - q transformation matrix is defined as:

$$[T_{dq0}(\theta_r)] = \frac{2}{3} \begin{bmatrix} \cos\theta_r & \cos\left(\theta_r - \frac{2\pi}{3}\right) & \cos\left(\theta_r + \frac{2\pi}{3}\right) \\ -\sin\theta_r & -\sin\left(\theta_r - \frac{2\pi}{3}\right) & -\sin\left(\theta_r + \frac{2\pi}{3}\right) \\ \frac{1}{2} & \frac{1}{2} & \frac{1}{2} \end{bmatrix} \quad (3.11)$$

and its inverse is given by

$$[T_{dq0}(\theta_r)]^{-1} = \begin{bmatrix} \cos\theta_r & -\sin\theta_r & 1 \\ \cos\left(\theta_r - \frac{2\pi}{3}\right) & -\sin\left(\theta_r - \frac{2\pi}{3}\right) & 1 \\ \cos\left(\theta_r + \frac{2\pi}{3}\right) & -\sin\left(\theta_r + \frac{2\pi}{3}\right) & 1 \end{bmatrix} \quad (3.12)$$

In Fig. 3.2, if the d - q axis is $\pi/2$ turned radian degrees Clock Wise (CW), the q - d transformation is obtained which is still considered a Park's Transformation as shown in Fig. 3.3. In the q - d transformation, the q -axis still leads the d -axis but angle representation is changed such that now θ is the rotor angle between the q -axis and a -axis which is chosen as a 0° reference for simplicity. q - d transformation is used to analyze the self and mutual inductances because of the ease of calculation. θ_r is considered as the actual rotor position (generally it can be obtained by using an encoder or similar position sensors) with respect to the a -axis which is used in the original Park's Transformation matrix, $[T_{dq0}(\theta_r)]$, but the angle depicted in Fig. 3.3, θ , which is between the q -axis and a -axis in q - d transformation does not represent the real rotor position. Therefore, the d -axis should be considered as a reference for measuring the real rotor angle with respect to 0° position selected as the a -axis in general. Eventually, the d - and q - axis synchronous inductances will be independent of the rotor position so that either of the transformations will give the same result.

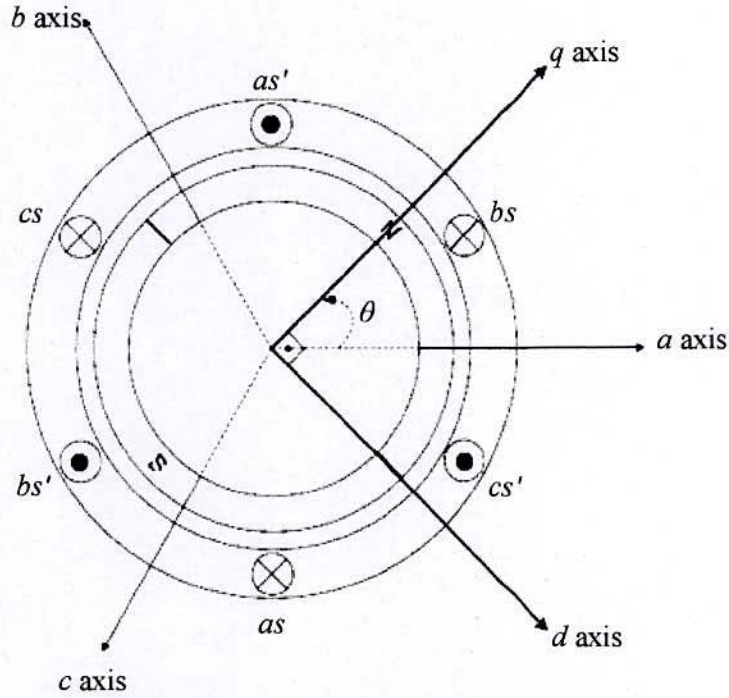


Figure 3.3 q -axis leading d -axis and the rotor angle represented as θ .

The Park's Transformation which has a d - q reference is of the form:

$$[f_{dq0}] = [T_{dq0}(\theta_r)][f_{abc}] \quad (3.13)$$

where f represents either a voltage, a current or a flux linkage; $[f_{dq0}] = [f_q, f_d, f_0]^t$,

$$[f_{abc}] = [f_a, f_b, f_c]^t.$$

The q - d transformation matrix is obtained as

$$[T_{dq0}(\theta)] = \frac{2}{3} \begin{bmatrix} \cos \theta & \cos\left(\theta - \frac{2\pi}{3}\right) & \cos\left(\theta + \frac{2\pi}{3}\right) \\ \sin \theta & \sin\left(\theta - \frac{2\pi}{3}\right) & \sin\left(\theta + \frac{2\pi}{3}\right) \\ \frac{1}{2} & \frac{1}{2} & \frac{1}{2} \end{bmatrix} \quad (3.14)$$

and the inverse of the above transformation matrix is given by

$$[T_{dq0}(\theta)]^{-1} = \begin{bmatrix} \cos \theta & \sin \theta & 1 \\ \cos\left(\theta - \frac{2\pi}{3}\right) & \sin\left(\theta - \frac{2\pi}{3}\right) & 1 \\ \cos\left(\theta + \frac{2\pi}{3}\right) & \sin\left(\theta + \frac{2\pi}{3}\right) & 1 \end{bmatrix} \quad (3.15)$$

Basically, if the rotor position θ is known, the above matrix transforms the variables of the stator reference frame to the one fixed to the rotor as shown in (3.13).

The relationship between θ and θ_r can be expressed with the help of Figs. 3.2 and 3.3 as

$$\theta = \theta_r + \frac{\pi}{2} \quad (3.16)$$

Equation (3.16) depicts that the actual rotor position, θ_r , is 90° (electrical degree) behind θ . If the q - d transformation matrix, $[T_{qd0}(\theta)]$, is used as a transformation matrix, the above description should be taken into account for deriving the q - d voltage equations of a PMSM.

If θ_r is known, the above formula can be substituted into the q - d transformation matrix $[T_{qd0}(\theta)]$ with the help of some trigonometric reduction equations shown below:

$$\begin{aligned} \cos\left(\theta_r + \frac{\pi}{2}\right) &= -\sin\theta_r \\ \sin\left(\theta_r + \frac{\pi}{2}\right) &= \cos\theta_r \end{aligned} \quad (3.17)$$

As a consequence of these manipulations, it has been observed that $[T_{qd0}(\theta)]$ and $[T_{dq0}(\theta_r)]$ are basically the same, except for the order of appearing of the d and q variables. One might say that $[T_{dq0}(\theta_r)]$ is more useful if no additional modification is wanted for assigning the actual rotor position, θ_r , as shown in Fig. 3.1.

Since L_{ss} is analyzed according to the q - d rotating reference frame, the corresponding relationship between flux linkages, $[\Lambda_{qd0}]$, the q - d axis currents, $[i_{qd0}]$, and the time-invariant q - d axis inductances, $[L_{qd0}]$, can be obtained by transforming only the stator quantities, that is:

$$[\Lambda_{qd0}] = [T_{qd0}(\theta)]L_{ss}[T_{qd0}(\theta)]^{-1}[i_{qd0}] + [T_{qd0}(\theta)][\Lambda_r] \quad (3.18)$$

where term $[T_{qd0}(\theta)]L_{ss}[T_{qd0}(\theta)]^{-1}$ is the transformation matrix which transforms the phase inductance matrix, L_{ss} , into the q - d axis synchronous inductance matrix, $[L_{qd0}]$. If the above description is applied to (3.18) then it can be shortened to:

$$[\Lambda_{qd0}] = [L_{qd0}][i_{qd0}] \quad (3.19)$$

by

$$\begin{aligned} [\Lambda_{qd0}] &= [\lambda_q, \lambda_d, \lambda_0]^T \\ [L_{qd0}] &= [L_q \quad L_d \quad L_0] \\ [i_{qd0}] &= [i_q, i_d, i_0]^T \end{aligned} \quad (3.20)$$

After simplifying the right hand side of (3.18), the rotor angle, θ_r , independent q - d axis flux linkages, λ_q and λ_d , synchronous inductances, L_q and L_d , and currents, i_q and i_d are obtained as follows:

$$\begin{aligned} \lambda_q &= \left(L_{ls} + \frac{3}{2}(L_0 - L_{ms}) \right) i_q = L_q i_q \\ \lambda_d &= \left(L_{ls} + \frac{3}{2}(L_0 + L_{ms}) \right) i_d + \lambda_r = L_d i_d + \lambda_r \\ \lambda_0 &= L_{ls} i_0 \quad (\text{zero in balanced systems}) \end{aligned} \quad (3.21)$$

where

$$\begin{aligned} L_q &= L_{ls} + L_{mq} \\ L_d &= L_{ls} + L_{md} \end{aligned} \quad (3.22)$$

In equation (3.22), L_{mq} and L_{md} are the common mutual inductances on the d -axis and q -axis circuits, respectively. Traditionally, the sums, $(L_{ls} + L_{mq})$ and $(L_{ls} + L_{md})$, are referred as the q -axis and d -axis synchronous inductances, respectively. Flux linkages in (3.20) can also be written as:

$$[\Lambda_{qd0}] = \begin{bmatrix} \lambda_q \\ \lambda_d \\ \lambda_0 \end{bmatrix} \quad (3.23)$$

On the contrary, flux linkages using the original Park's Transformation is differ from the above representation, $[\Lambda_{dq0}] = [\lambda_d, \lambda_q, \lambda_0]^T$. The only difference between $[\Lambda_{qd0}]$ and $[\Lambda_{dq0}]$ is the order of λ_q and λ_d . When λ_q and λ_d are known either $[\Lambda_{qd0}]$ or $[\Lambda_{dq0}]$ can be constructed easily. Once their components are known the transfer between each flux linkage matrix is easy.

So that (3.18) could have been written also as follows:

$$[\Lambda_{dq0}] = [T_{dq0}(\theta_r)]L_{ss}[T_{dq0}(\theta_r)]^{-1}[i_{dq0}] + [T_{dq0}(\theta_r)][\Lambda_r] \quad (3.24)$$

To collect the correct result out of the above equation, the rotor angle, θ , in the inductance matrix, L_{ss} , should be in the form of θ_r to be used in (3.24) by (3.16). After computing the above formula, the stator d - q axis flux linkages, λ_q and λ_d , will be the same as provided by (3.18). Results of the derivation of d - q axis stator flux linkages are given in (3.21).

The following part is the derivation of the d - q axis motor voltages of PMSM:

Equations (3.7) and (3.14) are the starting point. First, the original d - q Park's Transformation $[T_{dq0}(\theta_r)]$ is applied to the stator quantities shown in (3.7). This is given by:

$$\begin{aligned} [v_{dq0}] &= [T_{dq0}(\theta_r)][v_s] \\ [i_{dq0}] &= [T_{dq0}(\theta_r)][i_s] \\ [\Lambda_{dq0}] &= [T_{dq0}(\theta_r)][\Lambda_s] \end{aligned} \quad (3.25)$$

where

$$[v_{dq0}] = [v_d, v_q, v_0]^T \quad (3.26)$$

When the three-phase system is symmetrical and the voltages form a balanced three-phase set of abc sequences, the sum of the set is zero, hence the third components of the d - q quantities in (3.25) are zero, e.g. $v_0 = 0$.

If (3.25) is substituted into (3.7), then the stator voltage equation is written in d - q coordinates as:

$$[v_{dq0}] = [T_{dq0}(\theta_r)]r_s[T_{dq0}(\theta_r)]^{-1}[i_{dq0}] + [T_{dq0}(\theta_r)]p[T_{dq0}(\theta_r)]^{-1}[\Lambda_{dq0}] \quad (2.27)$$

where, p is the differential operator, $p = \frac{d}{dt}$.

In a three-phase balanced system, all the phase resistances are equal, $r_s = r_a = r_b = r_c$, such that the resistive drop term in the above equation reduces to

$$[T_{dq0}(\theta_r)]r_s[T_{dq0}(\theta_r)]^{-1}[i_{dq0}] = r_s[i_{dq0}] \quad (3.28)$$

The second term having a derivative part in (3.27) can be expanded as:

$$[T_{dq0}(\theta_r)]p[T_{dq0}(\theta_r)]^{-1}[\Lambda_{dq0}] = [T_{dq0}(\theta_r)]\left\{p[T_{dq0}(\theta_r)]^{-1}[\Lambda_{dq0}] + [T_{dq0}(\theta_r)]^{-1}p[\Lambda_{dq0}]\right\} \quad (3.29)$$

Further manipulations lead us to:

$$[T_{dq0}(\theta_r)]p[T_{dq0}(\theta_r)]^{-1}[\Lambda_{dq0}] = [T_{dq0}(\theta_r)]p[T_{dq0}(\theta_r)]^{-1}[\Lambda_{dq0}] + [T_{dq0}(\theta_r)][T_{dq0}(\theta_r)]^{-1}p[\Lambda_{dq0}] \quad (3.30)$$

and finally,

$$[T_{dq0}(\theta_r)]p[T_{dq0}(\theta_r)]^{-1}[\Lambda_{dq0}] = [T_{dq0}(\theta_r)]\left\{p[T_{dq0}(\theta_r)]^{-1}[\Lambda_{dq0}] + p[\Lambda_{dq0}]\right\} \quad (3.31)$$

where, the term $[T_{dq0}(\theta_r)]\left\{p[T_{dq0}(\theta_r)]^{-1}[\Lambda_{dq0}]\right\}$ is simplified as follows:

First, taking the derivative of (3.12), we get:

$$p[T_{dq0}(\theta_r)]^{-1} = \omega_r \begin{bmatrix} -\sin\theta_r & -\cos\theta_r & 0 \\ -\sin\left(\theta_r - \frac{2\pi}{3}\right) & -\cos\left(\theta_r - \frac{2\pi}{3}\right) & 0 \\ -\sin\left(\theta_r + \frac{2\pi}{3}\right) & -\cos\left(\theta_r + \frac{2\pi}{3}\right) & 0 \end{bmatrix} \quad (3.32)$$

where, ω_r is the rotor angular speed in electrical radians/sec, $\omega_r = \frac{d\theta_r}{dt}$. Multiplying

equations (3.11) and (3.32), we obtain:

$$[T_{dq0}(\theta_r)]\left\{p[T_{dq0}(\theta_r)]^{-1}\right\} = \omega_r \frac{2}{3} \begin{bmatrix} T_{11} & T_{12} & 0 \\ T_{21} & T_{22} & 0 \\ T_{31} & T_{32} & 0 \end{bmatrix} \quad (3.33)$$

where the elements of the matrix are written and manipulated by using some trigonometric reduction equations. The results are given below [26]:

$$\begin{aligned} T_{11} &= -\cos\theta_r \sin\theta_r - \cos\left(\theta_r - \frac{2\pi}{3}\right)\sin\left(\theta_r - \frac{2\pi}{3}\right) - \cos\left(\theta_r + \frac{2\pi}{3}\right)\sin\left(\theta_r + \frac{2\pi}{3}\right) = 0 \\ T_{12} &= -\cos^2\theta_r - \cos^2\left(\theta_r - \frac{2\pi}{3}\right) - \cos^2\left(\theta_r + \frac{2\pi}{3}\right) = -\frac{3}{2} \\ T_{21} &= \sin^2\theta_r + \sin^2\left(\theta_r - \frac{2\pi}{3}\right) + \sin^2\left(\theta_r + \frac{2\pi}{3}\right) = \frac{3}{2} \\ T_{22} &= \sin\theta_r \cos\theta_r + \sin\left(\theta_r - \frac{2\pi}{3}\right)\cos\left(\theta_r - \frac{2\pi}{3}\right) + \sin\left(\theta_r + \frac{2\pi}{3}\right)\cos\left(\theta_r + \frac{2\pi}{3}\right) = 0 \\ T_{31} &= -\frac{1}{2}\left\{\sin\theta_r + \sin\left(\theta_r - \frac{2\pi}{3}\right) + \sin\left(\theta_r + \frac{2\pi}{3}\right)\right\} = 0 \end{aligned} \quad (3.34)$$

$$T_{32} = -\frac{1}{2} \left\{ \cos \theta_r + \cos \left(\theta_r - \frac{2\pi}{3} \right) + \cos \left(\theta_r + \frac{2\pi}{3} \right) \right\} = 0$$

Putting all the elements obtained in (3.34) into (3.33), we get:

$$[T_{dq0}(\theta_r)] \left(p [T_{dq0}(\theta_r)]^{-1} \right) = \omega \frac{2}{3} \begin{bmatrix} 0 & -\frac{3}{2} & 0 \\ \frac{3}{2} & 0 & 0 \\ 0 & 0 & 0 \end{bmatrix} \quad (3.35)$$

More simplification leads us to:

$$[T_{dq0}(\theta_r)] \left(p [T_{dq0}(\theta_r)]^{-1} \right) = \omega \begin{bmatrix} 0 & -1 & 0 \\ 1 & 0 & 0 \\ 0 & 0 & 0 \end{bmatrix} \quad (3.36)$$

Equations (3.31) and (3.36) yield the following result, written in expanded matrix form:

$$\begin{bmatrix} v_d \\ v_q \\ v_0 \end{bmatrix} = r_s \begin{bmatrix} i_d \\ i_q \\ i_0 \end{bmatrix} + \omega_r \begin{bmatrix} 0 & -1 & 0 \\ 1 & 0 & 0 \\ 0 & 0 & 0 \end{bmatrix} \begin{bmatrix} \lambda_d \\ \lambda_q \\ \lambda_0 \end{bmatrix} + p \begin{bmatrix} \lambda_d \\ \lambda_q \\ \lambda_0 \end{bmatrix} \quad (3.37)$$

The above matrix can be arranged in equation form shown below:

$$\begin{aligned} v_d &= r_s i_d - \omega_r \lambda_q + p \lambda_d \\ &= r_s i_d - \omega_r L_q i_q + L_d p i_d \\ &= (r_s + L_d p) i_d - \omega_r L_q i_q \end{aligned} \quad (3.38)$$

Similarly,

$$\begin{aligned} v_q &= r_s i_q + \omega_r \lambda_d + p \lambda_q \\ &= r_s i_q + \omega_r L_d i_d + \omega_r \lambda_r + L_q p i_q \\ &= (r_s + L_q p) i_q + \omega_r (L_d i_d + \lambda_r) \end{aligned} \quad (3.39)$$

Equations (3.38) and (3.39) can be put together to form the famous d - q voltage model for the PMSM in matrix form. This is given in below:

$$\begin{bmatrix} v_d \\ v_q \end{bmatrix} = \begin{bmatrix} r_s + L_d p & -L_q \omega_r \\ L_d \omega_r & r_s + L_q p \end{bmatrix} \begin{bmatrix} i_d \\ i_q \end{bmatrix} + \lambda_r \omega_r \begin{bmatrix} 0 \\ 1 \end{bmatrix} \quad (3.40)$$

To obtain the d - q reference frame electromechanical torque, T_e , and the instantaneous input power P_i are used. Details are as follows:

Total input power P_i into the machine can be represented as

$$P_i = v_{sa}i_{sa} + v_{sb}i_{sb} + v_{sc}i_{sc} \quad (3.41)$$

When the stator phase quantities are transformed to the rotor d - q reference frame that rotates at a speed of $\omega_r = \frac{d\theta_r}{dt}$, (3.41) becomes:

$$P_i = \frac{3}{2}(v_q i_q + v_d i_d) \quad (3.42)$$

where the zero sequence quantities are neglected. Using (3.42), the mechanical output power P_o can be obtained by replacing v_d and v_q with the associated speed voltages as

$$P_o = \frac{3}{2}(-\omega_r \lambda_q i_d + \omega_r \lambda_d i_q) \quad (3.43)$$

For a P -pole machine, $\omega_r = (P/2)\omega_m$, where ω_m is the mechanical rotor speed in radians/sec, produced electromechanical torque T_e is derived when the output power P_o is divided by the mechanical speed ω_m , which is given as:

$$\begin{aligned} T_e &= \frac{3}{2} \frac{P}{2} (\lambda_d i_q - \lambda_q i_d) \\ &= \frac{3}{2} \frac{P}{2} ((L_d - L_q) i_q i_d + \lambda_r i_q) \end{aligned} \quad (3.44)$$

The torque balance equation for the motor speed dynamics is given

$$T_e = T_L + J_m p \omega_m + B_m \omega_m \quad (3.45)$$

It is apparent from (3.44) that the produced torque is composed of two distinct mechanisms. The first term corresponds to “reluctance torque” due to the saliency (difference in the d -axis and q -axis reluctance or inductance), while the second term corresponds to the “excitation torque” occurring between i_q and the permanent magnet λ_r .

3.3 Mathematical Model of 4S3P Inverter

The power circuit of the PMSM fed from 4S3P voltage source inverter is shown in Fig. 3.4. The circuit consists of two parts; first part is a front-end rectifier powered from single phase supply. The output dc voltage is smoothed through a two series connected capacitors. The second part of the power circuit is the three phase four switch inverter. The maximum obtainable peak value of the line voltages equals V_{dc} . In the analysis, the inverter switches are considered as ideal switches. The output voltages are defined by the gating signals of the two leg switches and by the two dc link voltages, V_{dc} .

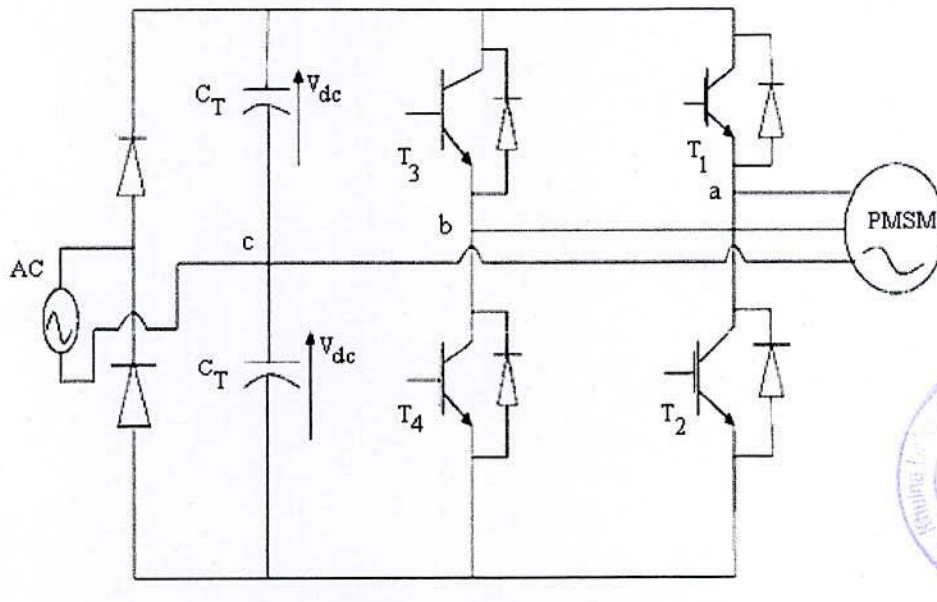


Figure 3.4 PMSM fed from a four switch inverter.

The phase voltage equations of the motor can be written as a function of the switching logic of the switches and the dc-link voltage V_{dc} [11] by

$$V_a = \frac{V_{dc}}{3} [4S_a - 2S_b - 1] \quad (3.46)$$

$$V_b = \frac{V_{dc}}{3} [4S_b - 2S_a - 1] \quad (3.47)$$

$$V_c = \frac{V_{dc}}{3} [-2S_a - 2S_b + 2] \quad (3.48)$$

where, V_a, V_b, V_c are inverter output voltages; V_{dc} is voltage across the dc link capacitors; S_a, S_b are switching function for each phase leg.

In matrix form the above equations can be written as

$$\begin{bmatrix} V_a \\ V_b \\ V_c \end{bmatrix} = \frac{V_{dc}}{3} \begin{bmatrix} 4 & -2 \\ -2 & 4 \\ -2 & -2 \end{bmatrix} + \frac{V_{dc}}{3} \begin{bmatrix} -1 \\ -1 \\ 2 \end{bmatrix} \quad (3.49)$$

For a balanced capacitor voltages, the four switching combinations lead to four voltage vectors as shown in Fig. 3.5 [11]. Table 3.1 shows the different mode of operation and the corresponding output voltage vector of the inverter. Fig. 3.6 shows the waveforms for the 3-phase voltages obtained from the inverter operation.

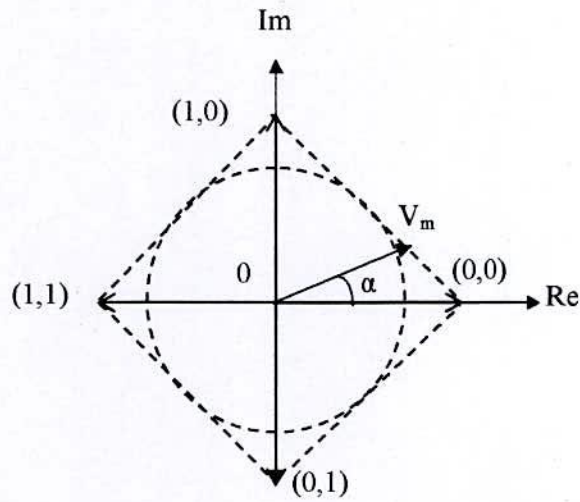


Figure 3.5 Switching vectors for a four switch inverter.

Table 3.1: Inverter Modes of Operation

Switching function		Switch on		Output voltage vector		
S_a	S_b			V_a	V_b	V_c
0	0	T_2	T_4	$-V_{dc}/3$	$-V_{dc}/3$	$2V_{dc}/3$
0	1	T_2	T_3	$-V_{dc}$	V_{dc}	0
1	0	T_1	T_4	V_{dc}	$-V_{dc}$	0
1	1	T_1	T_3	$V_{dc}/3$	$V_{dc}/3$	$-2V_{dc}/3$

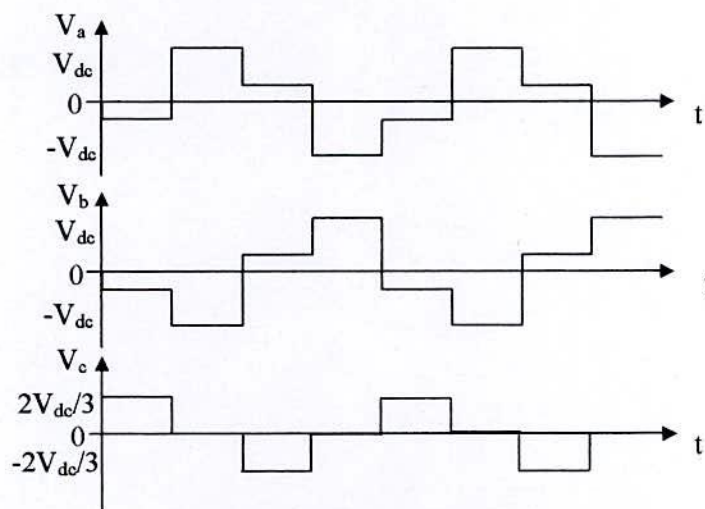


Figure 3.6 Waveforms for 3-phase voltages.

3.4 Controller Models

Automatic control has played a vital role in the advance of engineering and science. An automatic controller compare the actual value of the plant output with the reference input (desired value), determine the deviation and produces a control signal that will reduce the deviation to zero or to a small value. The manner in which the automatic controller produces the control signal is called control action.

3.4.1 PI Controller

A PI controller responds to an error signal in a closed control loop and attempts to adjust the controlled quantity to achieve the desired system response. The controlled parameter can be any measurable system quantity such as speed, torque, or flux. The benefit of the PI controller is that it can be adjusted empirically by varying one or more gain values and observing the change in system response. A digital PI controller is executed at a periodic sampling interval. It is assumed that the controller is executed frequently enough so that the system can be properly controlled. The error signal is formed by subtracting the desired setting of the parameter to be controlled from the actual measured value of that parameter. The sign of the error indicates the direction of change required by the control input. The Proportional (P) term of the controller is formed by multiplying the error signal by a P gain, causing the PI controller to produce a control response that is a function of the error magnitude. As the error signal become larger, the P term of the controller becomes larger to provide more correction. The effect of the P term tends to reduce the overall error as time elapses. However, the effect of the P diminishes as the error approaches zero. In most systems, the error of the controlled parameter gets very close to zero but does not converge. This results in a small remaining steady state error. The Integral (I) term of the controller is used to eliminate the steady state errors. The I term calculates a continuous running total of the error signal. Therefore, a small steady state error accumulates into a large error value over time. This accumulated error signal is multiplied by an I gain factor and becomes the I output term of the PI controller.

For a controller with proportional control action, the value of the controller output $u(t)$ is proportional to the actuating error signal $e(t)$. That is,

$$u_p(t) = K_p e(t) \quad (3.50)$$

For a controller with integral action, the value of the controller output $u(t)$ is changed at a rate proportional to the actuating error signal $e(t)$. That is,

$$u_i(t) = K_i \int_0^t e(t) dt \quad (3.51)$$

PI controller combines the function of proportional and integral controllers. So, in case of PI control action, the controller output will be,

$$u(t) = K_p e(t) + K_i \int_0^t e(t) dt \quad (3.52)$$

From (3.52) we get by Laplace transformation

$$\frac{U(s)}{E(s)} = K_p + \frac{K_i}{s} \quad (3.53)$$

The block diagram of a PI controller is shown in Fig. 3.7.

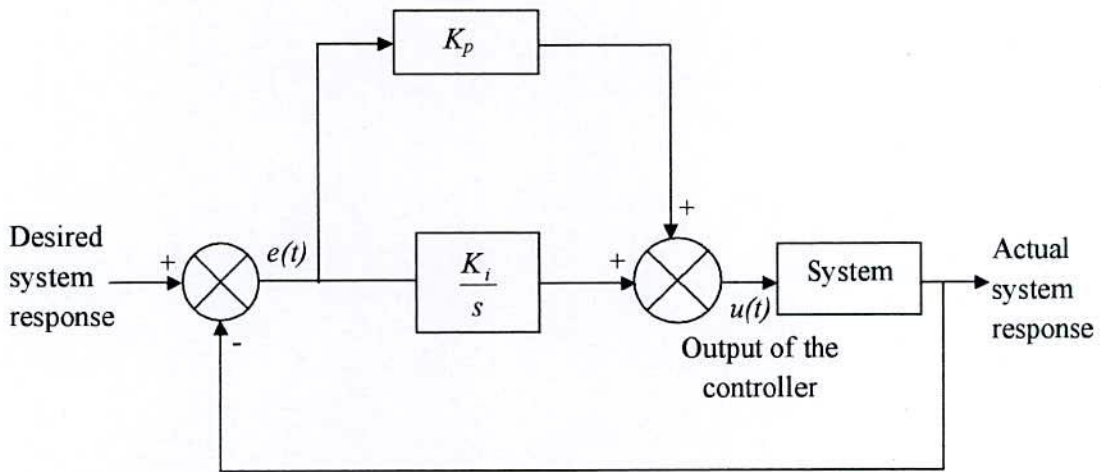


Figure 3.7 Block diagram of a PI controller.

3.4.2 Hysteresis Current Controller

The hysteresis modulation is a feedback current control method where the motor current tracks the reference current within a hysteresis band. Hysteresis current controller can be implemented to control the inverter currents. The controller will generate the reference currents with the inverter within a range which is fixed by the width of the band gap. In this controller the desired current of a given phase is summed with the negative of the measured current. The error is fed to a comparator having a hysteresis band. If the current

exceeds the upper limit of the hysteresis band, the upper switch of the inverter arm is turned off and the lower switch is turned on. Therefore, the current starts to decay. If the current crosses the lower limit of the hysteresis band, the lower switch of the inverter arm is turned off and the upper switch is turned on. As a result, the current gets back into the hysteresis band. Hence, the actual current is forced to track the reference current within the hysteresis band. Fig. 3.8 shows the hysteresis band with the actual current and the resulting gate signals.

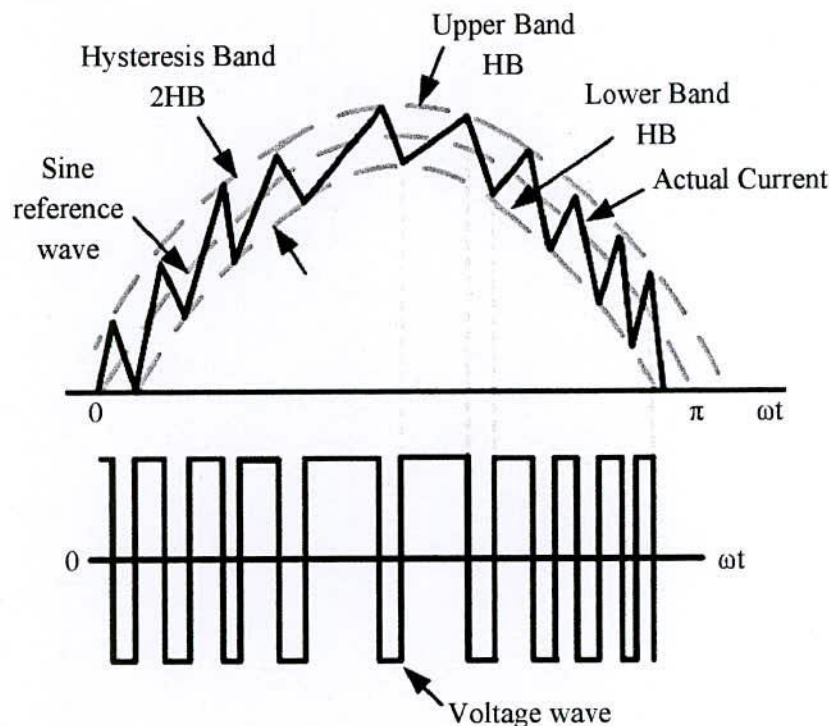


Figure 3.8 Hysteresis controller.

3.5 Conclusion

In this chapter, mathematical models of PM machines are established in both stationary reference frame and the rotating reference frame with respect to the PM motors with and without saliency, e.g., IPM and SPM. By using the Park's transformation, all time-varying inductances in the voltage equations are eliminated and in turn the models are simplified and vector control algorithms can be implemented. Using the 4S3P inverter model, the equations of the supplied voltage to the motor is obtained. Besides, control techniques of PI controller and hysteresis current controller are discussed clearly.

CHAPTER IV

Artificial Neural Network and Proposed Control System

4.1 Introduction

High performance drive systems using PMSM drives require the instantaneous knowledge of the positions of rotating phase variables. For field orientation, stator flux magnitude and rotor position information are very important to implement the control laws. There are several methods reported in the literature to estimate the stator flux magnitude and position accurately and robustly. In this study Artificial Neural Network (ANN) based stator flux estimator is proposed. A brief discussion on ANN's and their Real Time Recurrent Learning (RTRL) method are described at the beginning of this chapter. Finally, description on the proposed PMSM control scheme will be presented.

4.2 Artificial Neural Network

An ANN is an information processing paradigm that is inspired by the way biological nervous systems work, such as the brain processes information [31]. The key element of this paradigm is the novel structure of the information processing system. It is composed of a large number of highly interconnected processing elements (neurons) working in unison to solve specific problems. ANN's like human beings, learn by example. An ANN is configured for a specific application, such as pattern recognition or data classification, through a learning process. Learning in biological systems involves adjustments to the synaptic connections that exist between the neurons. This is true for ANN's as well. The use of neural networks offers the following useful properties and capabilities:

- Nonlinearity
- Input-output mapping
- Adaptivity
- Evidential response
- Contextual information
- Fault tolerant
- VLSI implementation
- Uniformity in analysis and design
- Neurobiological analogy

4.2.1 Models of a Neuron

A neuron is an information-processing unit that is fundamental to the operation of a neural network. The block diagram of Fig. 4.1 shows the model of a neuron [31], which forms the basis for designing (artificial) neural networks. Here we identify three basic elements of the neuronal model:

- A set of **synapses** or connecting links, each of which is characterized by a weight or strength of its own. Specifically, a signal x_j at the input of synapse j connected to the neuron k is multiplied by the synaptic weight w_{kj} . It is important to make a note of the manner in which the subscripts of the synaptic weight w_{kj} are written. The first subscript refers to the neuron in question and the second subscript refers to the input end of the synapse to which the weight refers. Unlike a synapse in the brain, the synaptic weights of an artificial neuron lie in a range that includes negative as well as positive values.
- An **adder** for summing the input signals, weighted by the respective synapses of the neuron; the operations described here constitutes a linear combiner.
- An **activation function** for limiting the amplitude of the output of a neuron. The activation function is also referred to as a squashing in that it squashes (limits) the permissible amplitude range of the output signal to some finite value.

The neuronal model of Fig. 4.1 also includes an externally applied *bias*, denoted by b_k that has the effect of increasing or lowering the net input of the activation function, depending on whether it is positive or negative, respectively.

In mathematical terms; a neuron k is written by the following pair of equations:

$$u_k = \sum_{j=1}^m w_{kj} x_j \quad (4.1)$$

and

$$y_k = \varphi(u_k + b_k) \quad (4.2)$$

where, $x_1, x_2, \dots, \dots, x_m$ are the input signals, $w_{k1}, w_{k2}, \dots, \dots, w_{km}$ are the synaptic weights of neuron k , u_k is the linear combiner output due to the signals, b_k is the bias, $\phi(\cdot)$ is the activation function and y_k the output signal of the neuron.

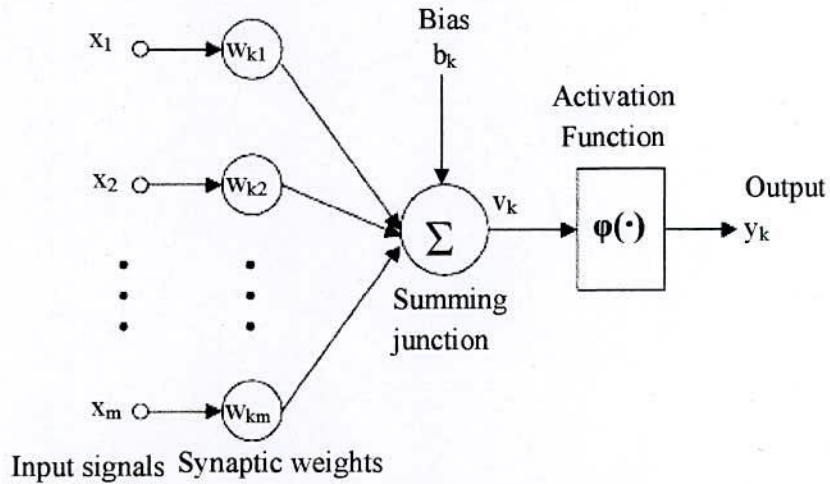


Figure 4.1 Nonlinear model of a neuron.

The use of bias b_k has the effect of applying an affine transformation to the output u_k of the linear combiner in the model of Fig. 4.1, as shown by:

$$v_k = u_k + b_k \tag{4.3}$$

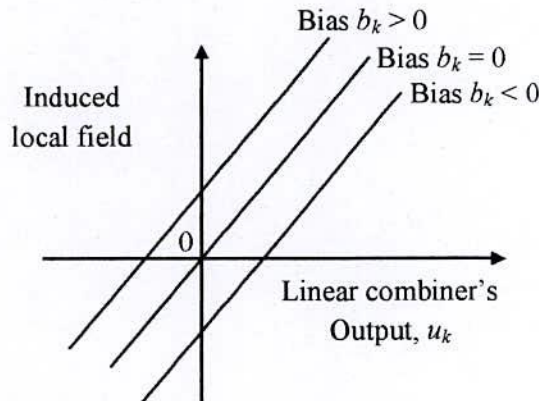


Figure 4.2 Affine transformations produced by the presence of a bias;

where $v_k = b_k$ at $u_k = 0$.

In particular, depending on whether the bias b_k is positive or negative, the relationship between the induced local field or activation potential v_k of neuron k and the linear

combiner output u_k is modified in the manner will be illustrated later; hereafter the term “induced local field” is used. It can be noted that as a result of this affine transformation, the graph of v_k verses u_k no longer passes through the origin. The bias is external parameters of artificial neuron k . We may account for its presence as in (4.2). Equivalently, we may formulate the combination of (4.1) to (4.3) as follows:

$$v_k = \sum_{j=0}^m w_{kj} x_j \quad (4.4)$$

and $y_k = \varphi(v_k)$ (4.5)

In (4.4) we have added a new synapse. Its input is:

$$x_0 = +1 \quad (4.6)$$

and its weight is:

$$w_{k0} = b \quad (4.7)$$

We may therefore reformulate the model of neuron k as in Fig. 4.3.

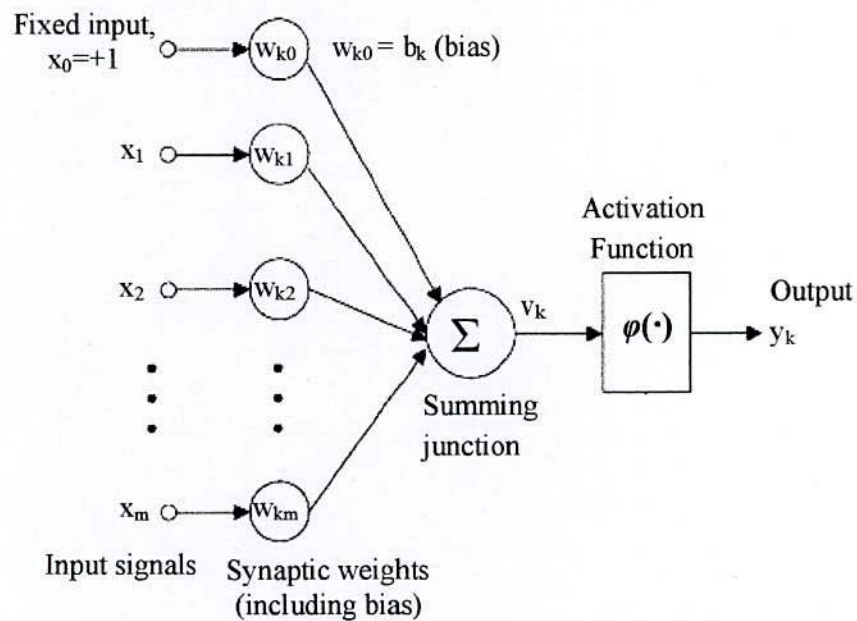


Figure 4.3 Another nonlinear model of a neuron.

In this figure, the effect of the bias is accounted for by doing two view points:

- (1) Adding a new input signal fixed at +1, and
- (2) Adding a new synaptic weight equal to the bias b_k .

Although the models of Figs. 4.1 and 4.3 are different in appearance, they are mathematically equivalent.

4.2.2 Real Time Recurrent Learning Algorithm

The property that is of primary significance for a neural network is the ability of the network to learn from environment, and to improve its performance through learning. A neural network learns from its environment through an interactive process of adjustments applied to its synaptic weights and bias levels. Ideally, the network becomes more knowledgeable about its environment after every iteration of learning process. The definition of learning in the context of neural network is [31]: "Learning is a process by which the free parameters of a neural network are adapted through a process of simulation by the environment in which the network is embedded. The type of learning is determined by the manner in which the change of parameters takes place."

The RTRL algorithm derives its name from the fact that adjustments are made to the synaptic weights of a fully connected recurrent network in real time. Fig. 4.4 shows the layout of such a recurrent network [31].

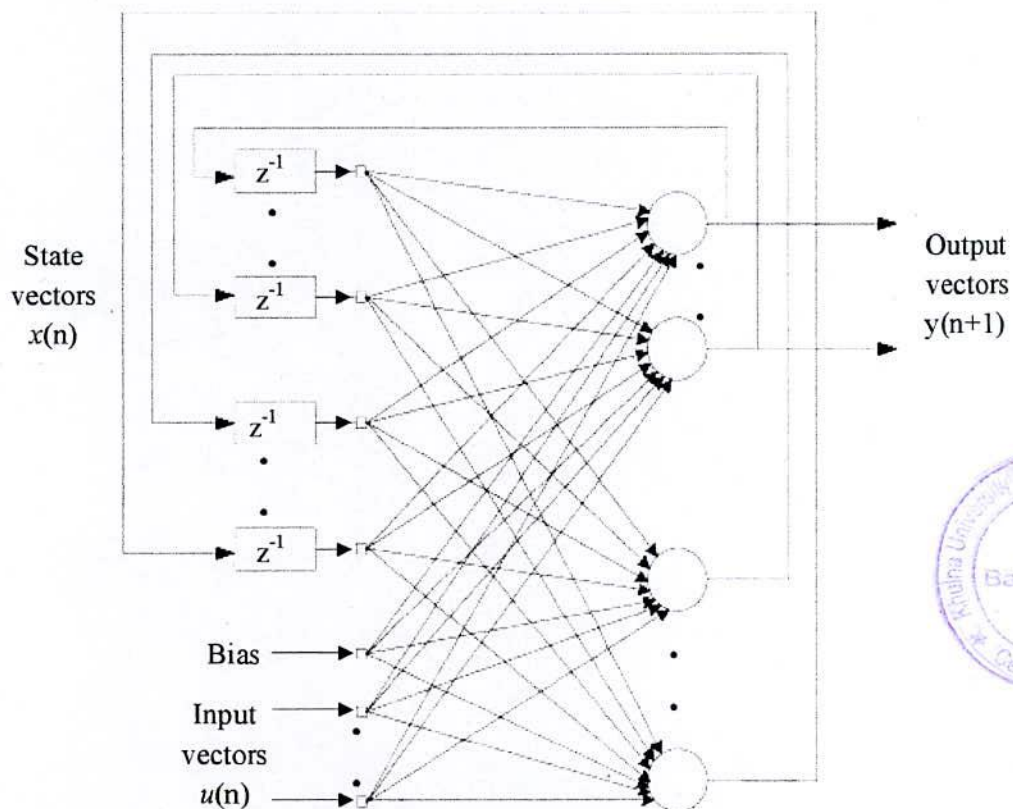


Figure 4.4 Fully connected real time recurrent network.

In mathematical terms, the dynamical behavior of any noise free system can be described by the following pair of nonlinear equations:

$$x(n+1) = \varphi(W_a x(n) + W_b u(n)) \quad (4.8)$$

$$y(n) = Cx(n) \quad (4.9)$$

where, $x(n)$ is the q -by- 1 nonlinear state matrix, $u(n)$ is m -by- 1 input matrix, $y(n)$ is the p -by- 1 corresponding output matrix, W_a is the q -by- q matrix, W_b is the q -by- $(m+1)$ matrix, and C is the p -by- q matrix.

The process equation (4.8) in the state-space description of the network is written in the following form:

$$x(n+1) = \begin{bmatrix} \varphi(W_1^T \xi(n)) \\ \bullet \\ \bullet \\ \varphi(W_j^T \xi(n)) \\ \bullet \\ \bullet \\ \varphi(W_q^T \xi(n)) \end{bmatrix} \quad (4.10)$$

It is assumed that all the neurons have a common activation function $\varphi(\cdot)$. The $(q+m+1)$ -by- 1 vector w_j is the synaptic weight vector of neuron j in the recurrent network, that is:

$$w_j = \begin{bmatrix} w_{a,j} \\ w_{b,j} \end{bmatrix}, j = 1, 2, \dots, q \quad (4.11)$$

where, $w_{a,j}$ and $w_{b,j}$ are the j th columns of the transposed weight matrices W_a^T and W_b^T respectively. The $(q+m+1)$ -by- 1 vector:

$$\xi(n) = \begin{bmatrix} x(n) \\ u(n) \end{bmatrix} \quad (4.12)$$

The last elements of $u(n)$ is $+1$ and, in a corresponding way, the first element of $w_{b,j}$ is equal to the bias b_j applied to neuron j .

The q -by- $(q+m+1)$ partial derivative matrix of the state vector $x(n)$ with respect to the weight vector w_j :

$$\Lambda_j(n) = \frac{\partial x(n)}{\partial w_j(n)}, j = 1, 2, \dots, q \quad (4.13)$$

$U_j(n)$ is a q -by- $(q+m+1)$ matrix whose rows are all zero, except for the j th row that is equal to the transpose of vector $\xi^T(n)$:

$$U_j(n) = \begin{bmatrix} 0^T \\ \xi^T(n) \\ 0^T \end{bmatrix} \leftarrow j\text{th row } j = 1, 2, \dots, q \quad (4.14)$$

$\varphi(n)$ is a q -by- q diagonal matrix whose k th diagonal element is the partial derivative of the activation function with respect to its arguments, evaluated at $w_j^T \xi(n)$:

$$\varphi(n) = \text{diag} \left[\varphi'(W_1^T \xi(n)), \varphi'(W_2^T \xi(n)), \dots, \varphi'(W_q^T \xi(n)) \right] \quad (4.15)$$

With these definitions, the following recursive equation Λ_j for the neuron j can be obtained by differentiating (4.10) with respect to w_j and using the chain rule of calculus:

$$\Lambda_j(n+1) = \varphi(n) [W_a(n) \Lambda_j(n) + U_j(n)], \quad j = 1, 2, \dots, q \quad (4.16)$$

The objective of the learning process is to minimize a cost function obtained by the instantaneous sum of squared errors at time n , which is defined in terms of $e(n)$ by

$$\xi(n) = \frac{1}{2} e^T(n) e(n) \quad (4.17)$$

where the p -by- 1 error vector $e(n)$ is defined by using the measurement equation:

$$e(n) = \tilde{y}(n) - y(n) \quad (4.18)$$

where $\tilde{y}(n)$ denotes the desired output vector. The adjustment for the weight vector of the j th neuron, ΔW_j , is:

$$\Delta W_j = -\eta \frac{\partial \xi(n)}{\partial W_j(n)} = \eta C \Lambda_j(n) e(n), \quad j = 1, 2, \dots, q \quad (4.19)$$

4.2.3 Proposed Stator Flux Estimation Methodology

The main problem of the integration in flux estimation as used in high performance electrical drives is the presence of dc biases which affect the accuracy of the flux estimation [32]. In particular dc drifts are always present in the signal before it is integrated, which causes the integrator to saturate with a resulting inadmissible estimation error. Moreover, a dc bias also appears at the output of the integrator because of the initial

conditions. Then it is necessary to filter the dc components of the signals both before and after it is integrated, without being affected by those errors which arise at low frequencies when LP filters are used. The idea is then to use an adaptive filter used as a notch filter to cut off the dc component adaptively. The use of a fixed notch filter is here infeasible essentially because it would be too complex and computationally cumbersome, while the adaptive filter here used is very simple. On the other hand, the adaptation time is not at all critical for the application under study.

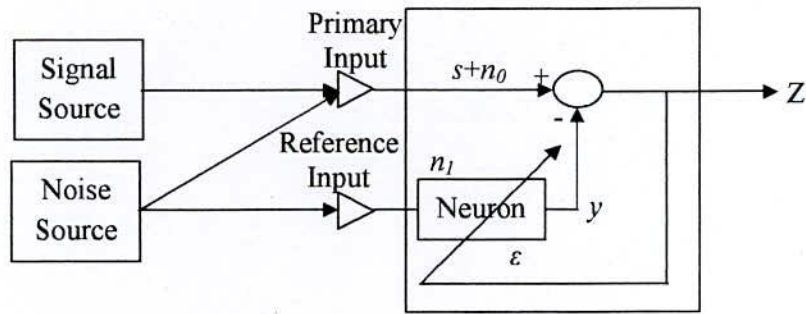


Figure 4.5 Block diagram of neural network filter.

Fig. 4.5 shows the block diagram of a neural filter or adaptive noise canceller, as called in [33]. The input signal is the signal affected from noise, and it can be considered as $s+n_0$ where s is the signal and n_0 is the noise, uncorrelated with the signal. This input signal $s+n_0$ is the so-called “primary input” to the neural filter. Let then a second noise n_1 be received by the neural filter and let this noise be also uncorrelated with s , but in a way correlated with n_0 . This second noise is the so-called “reference input” to the neuron. The noise n_1 is given as input to the neuron and the output y is then subtracted to the primary input so as to obtain the system output $z = s + n_0 - y$, which is also the error ε between the primary input and y . The reference input is processed by the linear neuron by a least-squares algorithm in order to minimize the total power output $E[\varepsilon^2]$ where $E[\cdot]$ is the expectation function. This goal is reached by feeding back the output signal z to the linear neuron. If this minimization is reached, then also $E[(n_0 - y)^2]$ is minimized as the signal power $E[s^2]$ is not affected. This is the same as approximating s with ε in a least squares sense. Consequently, the minimization of the total power output implies the maximization of the output signal-to-noise ratio. It must be emphasized that only an approximate correlation

between the noises n_a and n_o is necessary, and nothing more. In the case of the problem at hand, the noise n_o is the dc component. So a notch filter with a notch at zero frequency can be achieved if a neuron with only one bias weight is used, i.e., a neuron whose input is a constant, e.g., -1.

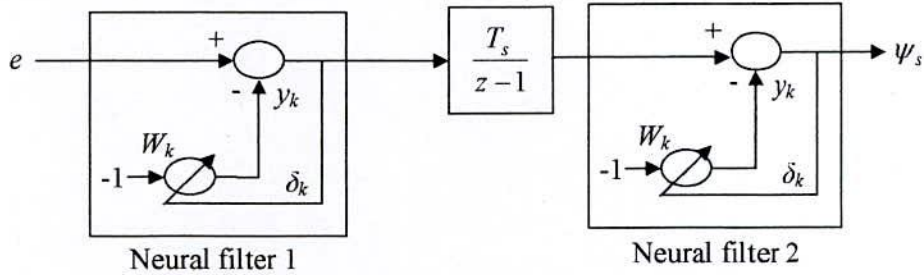


Figure 4.6 Neural filter based integrator.

Fig. 4.6 shows the adaptive integrator with two identical neural notch filters before and after the pure integrator. The learning law of the neural adaptive filter is then

$$y_{k+1} = y_k + 2\mu\epsilon_k = y_k + 2\mu(d_k - y_k) \quad (4.20)$$

where k is the actual time constant, d_k is either e (in the first notch filter) or the output of the integrator (in the second notch filter) and μ is the learning rate. This signal weight neuron is able to remove not only a constant bias but also a slowly varying drift in the primary input [33]. It should be remarked that two neural filters must be used in the neural based integrator: the neural filter 1 eliminates the dc component of the signal to be processed, the neural filter 2 eliminates the dc drift appearing at the output of the integrator because of the initial conditions and of the filtering error of the neural filter 1 during its adaptation. The linear neuron based integration method will also be compared with another neural integrator developed. In neural integration algorithm the flux-linkage ψ is obtained from emf e by an integration method accomplished by a Programmable Cascaded Low Pass Filter (PCLPF) implemented by a hybrid neural network consisting of a Recurrent Neural Network (RNN) and a feed-forward artificial neural network. Here only the fundamentals are described, in accordance with [34], if two identical low-pass filters are cascaded (PCLPF), transfer functions in the z -domain given by

$$\frac{\psi_1(z)}{E(z)} = \frac{Kz^{-1}}{1 - \alpha z^{-1}} \quad \text{and} \quad \frac{\psi(z)}{\psi_1(z)} = \frac{Kz^{-1}}{1 - \alpha z^{-1}} \quad (4.21)$$

where $E(z)$, $\psi_1(z)$, $\psi(z)$ are, respectively, the z-transforms of the input signal $e(k)$, the output of the first filter $\psi_1(k)$ and the output of the second filter $\psi(k)$, $\alpha = 1 - \frac{T_s}{\tau}$, T_s is the sampling time, τ the time constant of each component filter, $K = \left(\frac{T_s}{G}\right) / \tau$, G is the amplitude of the compensation gain of the PCLPF.

An equivalent RNN is then suggested which results in the following matrix equation:

$$\begin{bmatrix} \lambda_{as}(k+1) \\ \lambda_{\beta s}(k+1) \end{bmatrix} = \begin{bmatrix} W_{11} & W_{12} \\ W_{21} & W_{22} \end{bmatrix} \begin{bmatrix} \lambda_{as}(k) \\ \lambda_{\beta s}(k) \end{bmatrix} + \begin{bmatrix} W_{13} \\ W_{23} \end{bmatrix} i_{as}(k) + \begin{bmatrix} W_{14} \\ W_{24} \end{bmatrix} i_{\beta s}(k) + \begin{bmatrix} W_{15} \\ W_{25} \end{bmatrix} E_{\omega}(k) \quad (4.22)$$

$$\text{Estimated angle, } \theta = \tan^{-1} \left(\frac{\lambda_{\beta s}}{\lambda_{as}} \right) \quad (4.23)$$

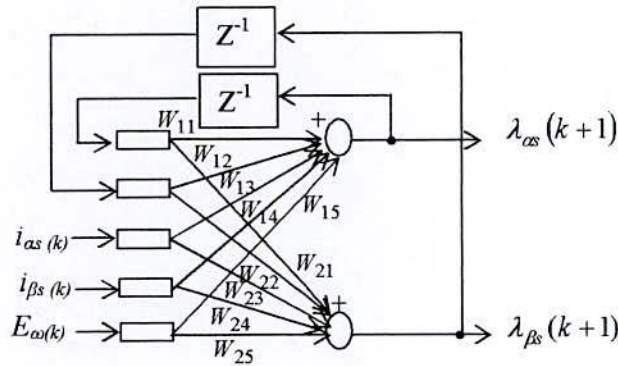


Figure 4.7 Stationary α - and β -axis stator flux estimation by CRTRL algorithm.

where W_{11} , W_{12} , W_{21} , W_{22} , etc are the weights of the RNN, which is shown in Fig. 4.7. The RNN weights are dependent on the sampling frequency of the control system: this means that a retraining of the RNN is required if the sampling frequency varies.

4.3 Proposed PMSM Control Scheme

The proposed vector control scheme is shown in Fig. 4.8. The speed error (E_{ω}) is processed through a PI controller to generate the torque producing component of the stator current (i_t^*). The magnetizing component of the stator current (i_m^*) is obtained from flux program.

i_m^* and i_t^* are then used to generate the reference currents i_a^* and i_b^* . The rotor angle required for vector rotation is obtained from RNN based flux and position estimator. Two independent hysteresis current controllers with a suitable hysteresis band are used to command the motor currents i_a , and i_b to follow the reference currents. The hysteresis controllers also generate four switching signals which fires the power semiconductor devices of the three phase inverter to produce the actual voltages to the motor. The three phase motor currents i_a , i_b , and i_c are transformed into α -, and β -axis components through Clarke's transformation. A speed transducer is used to measure the speed of the PMSM accurately.

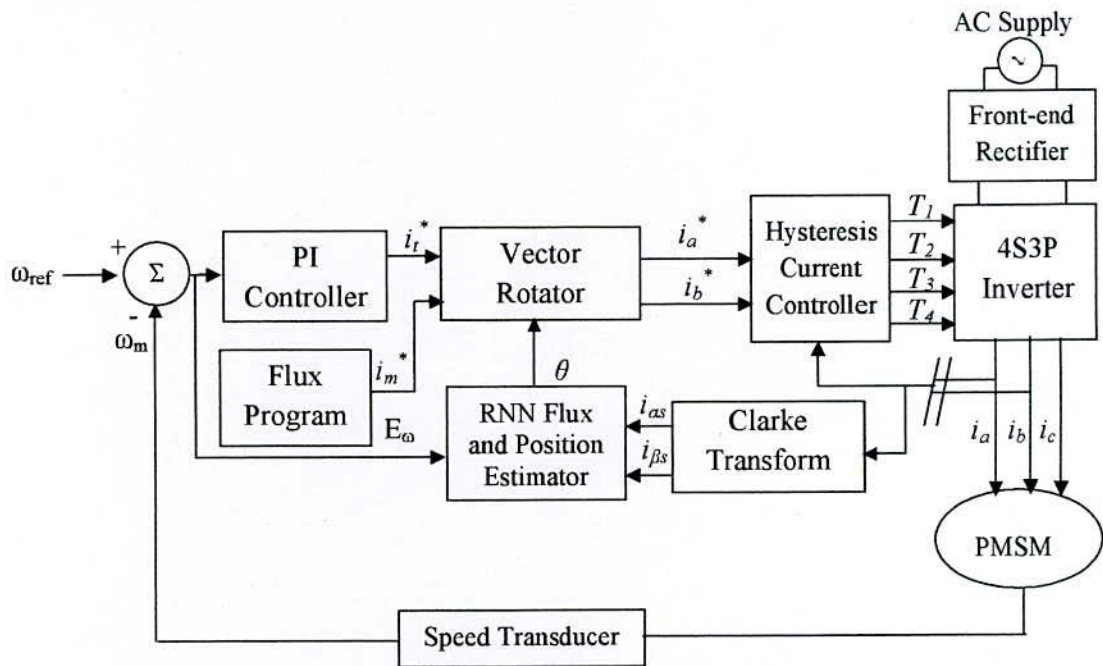


Figure 4.8 Proposed control scheme of the PMSM.

4.3.1 Adjusting the PI Gains

When tuning a PI controller for first time, the I gain is set to zero. Then the P gain is increased until the system responds well to set point changes without excessive overshoot or oscillations. Using lower values of P gain will 'loosely' control the system, while higher values will give 'tighter' control. At this point, the system will probably not converge to the set point. After selecting a reasonable value of P gain, the I gain is increased slowly to force the system error to zero. Only a small amount of I gain is required in most systems.

The effect of I gain, if large enough, can overcome the action of the P term, slow the overall control response and cause the system to oscillate around the set point. If oscillation occurs, reducing the I gain and increasing the P gain will usually solve the problem. There is a single PI control loop in this application. The selection of suitable values for gain constants is carried out for different combinations of K_p and K_i after having their initial guesses following the ideas in [35].

4.3.2 Flux Program

In constant-torque region the torque can be controlled by i_t whereas stator flux (λ_s) can be maintained at a value determined by the flux program. The proposed control system incorporates a flux control loop where the stator flux command (λ_s^*) is generated through the flux program. The flux loop then generates magnetizing component of the stator current (i_m^*) and helps maintaining the desired λ_s irrespective of parameter variation effect.

4.3.3 Coordinate Transforms

4.3.3.1 Vector Rotator

The first coordinate transform, called the vector rotator, moves a two axis, two dimensional coordinate system, referenced to the stator, onto a three axis system, keeping the same reference. In this application, the command i_m^* and i_t^* signals are processed through vector rotator to generate the three phase current commands for the hysteresis current controller. The stationary axes a -, b -, c -, their two phase equivalents α -, β -, and the rotating axes of the PMSM are shown in Fig. 4.9.

The reference currents are formulated as follows:

$$i_a^* = i_m^* \cos \theta - i_t^* \sin \theta \quad (4.24)$$

$$i_b^* = i_m^* \cos(\theta - 120^\circ) - i_t^* \sin(\theta - 120^\circ) \quad (4.25)$$

$$i_c^* = i_m^* \cos(\theta + 120^\circ) - i_t^* \sin(\theta + 120^\circ) \quad (4.26)$$

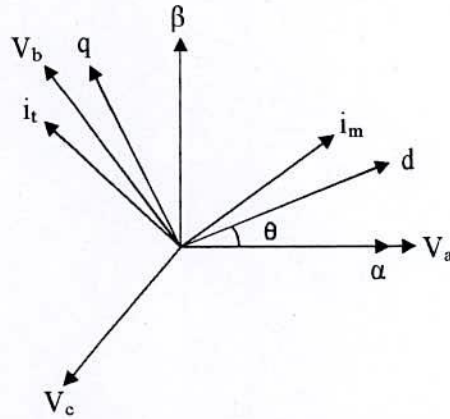


Figure 4.9 Stationary and rotating axes of PMSM.

4.3.3.2 Clarke Transform

The Clarke transform converts the stationary 3-axes (a -, b -, c -) quantities to stationary 2-axes (α -, β -) quantities by the following equations:

$$i_{\alpha s} = i_a - \frac{1}{2}i_b - \frac{1}{2}i_c \quad (4.27)$$

$$i_{\beta s} = \frac{\sqrt{3}}{2}(i_b - i_c) \quad (4.28)$$

4.3.4 Hysteresis Current Control Technique

The main task of the current controller is to force the current vector in the three phase load according to a reference trajectory. The block diagram of a three-phase hysteresis current controller is shown in Fig. 4.10. The scheme compares the phase currents with the desired values within the Hysteresis Band (HB) to take decision on switching of inverter transistor.

The switching logics are formulated as given below:

if $i_a < (i_a^* - \text{HB})$ T₁ on and T₂ off

if $i_a > (i_a^* + \text{HB})$ T₁ off and T₂ on

if $i_b < (i_b^* - \text{HB})$ T₃ on and T₄ off

if $i_b > (i_b^* + \text{HB})$ T₃ off and T₄ on

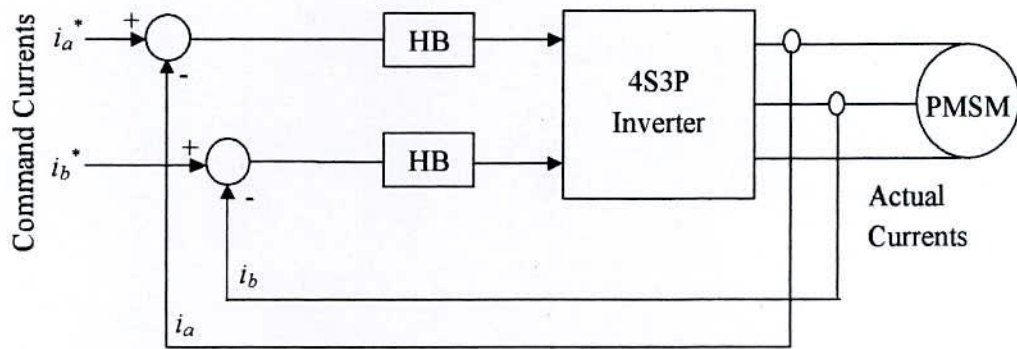


Figure 4.10 Hysteresis current controller block diagram.

4.4 Conclusion

In this chapter an idea concerning position sensorless control has been presented. The aim of this research was to find a position estimation scheme for the PMSM that is capable of working under all operating conditions, i.e. from zero to high speed and zero to full load. Therefore, a RNN based stator flux and rotor position estimator is proposed. Beside this, the application of PI controller and hysteresis current controller in the vector control of the PMSM drive is described briefly.



CHAPTER V

Simulation Results and Discussions

5.1 Introduction

This chapter deals with the simulation results of the PMSM drive system. A simulation study is conducted in order to test the performance of the drive system. The system under consideration is simulated in C++ environment. The machine model is considered in d - q axes frame. The state space equations are solved with Runge-Kutta-Gill subroutine. The sampling time for simulating the system is $5 \mu\text{s}$. Reference phase currents are generated from the torque and magnetizing currents i_t^* and i_m^* . The phase voltages V_a , V_b , and V_c resulting from the hysteresis current controller are transformed into d - and q -axis quantities V_d and V_q . Currents obtained from simulation model are transferred to get the actual phase currents. The rating and motor parameters used in this simulation are given in Appendix. The simulation results for different operating conditions are listed in the subsequent sections.

5.2 RNN based Stator Flux and Rotor Position Estimation

The effectiveness of the proposed flux estimator along α - β axes needs to be verified before implementing it in the drive system. The weights of the RNN are obtained by training the neural network by CRTRL algorithm and are provided in Appendix. Real time flux components calculated from exact values of motor variables are computed and compared with the estimated flux components. Figs. 5.1.1 and 5.1.2 give a comparison between the actual and estimated values of α - β axes stator fluxes and rotor angle for the 4S3P inverter fed drive under transient and steady-state conditions when the motor runs at 1500 rpm. Fig. 5.1.3 gives a comparison between the actual and estimated values of the stator fluxes and rotor angle for the 4S3P inverter fed drive when the motor runs at 150 rpm. A complete matching of the variables is indicated in the figures. The performance of the RNN estimator is also investigated for 6S3P inverter fed PMSM drive. Fig. 5.2.1 to Fig. 5.2.3 show the estimated and actual values of α - β axes stator fluxes and rotor angle for the 6S3P

inverter fed drive. Clearly, the proposed RNN estimator can be used to accurately estimate stator flux components and rotor angle at both high- and low-motor speeds.

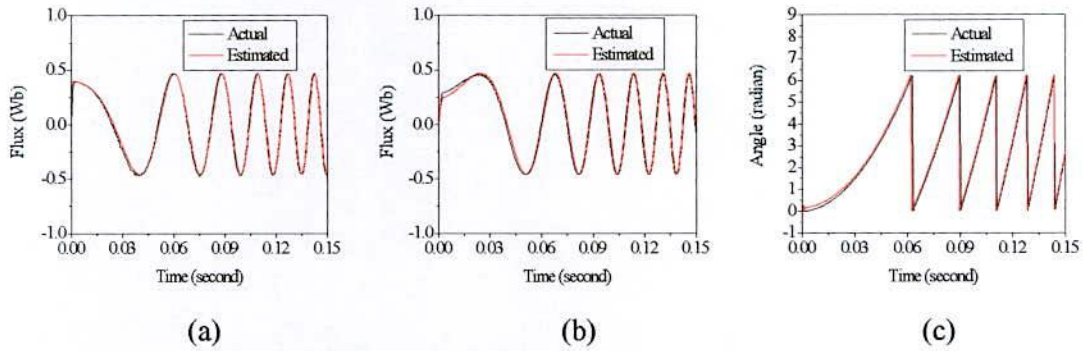


Figure 5.1.1 Actual and estimated responses of (a) α -axis stator flux, (b) β -axis stator flux, and (c) Rotor angle for the 4S3P inverter fed PMSM drive (runs at 1500 rpm) under transient condition.

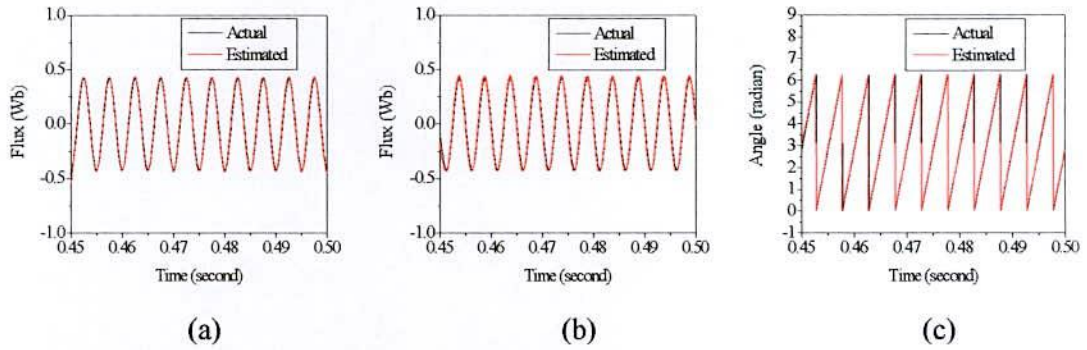


Figure 5.1.2 Actual and estimated responses of (a) α -axis stator flux, (b) β -axis stator flux, and (c) Rotor angle for the 4S3P inverter fed PMSM drive (runs at 1500 rpm) under steady-state condition.

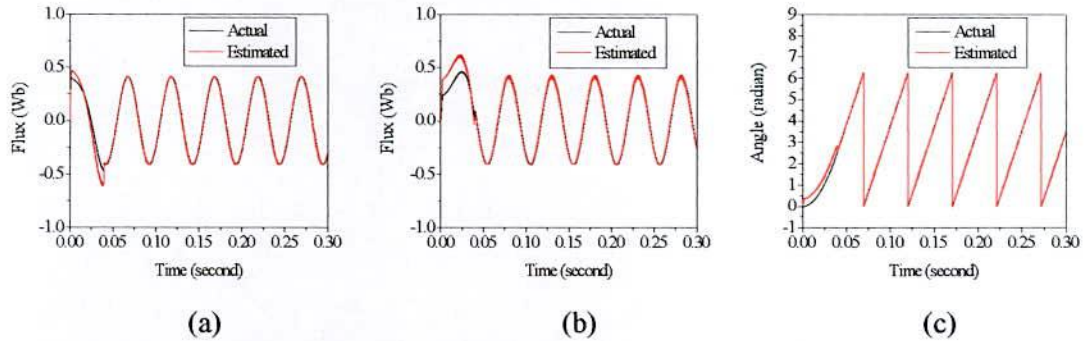


Figure 5.1.3 Actual and estimated responses of (a) α -axis stator flux, (b) β -axis stator flux, and (c) Rotor angle for the 4S3P inverter fed PMSM drive (runs at 150 rpm) under transient and steady-state conditions.

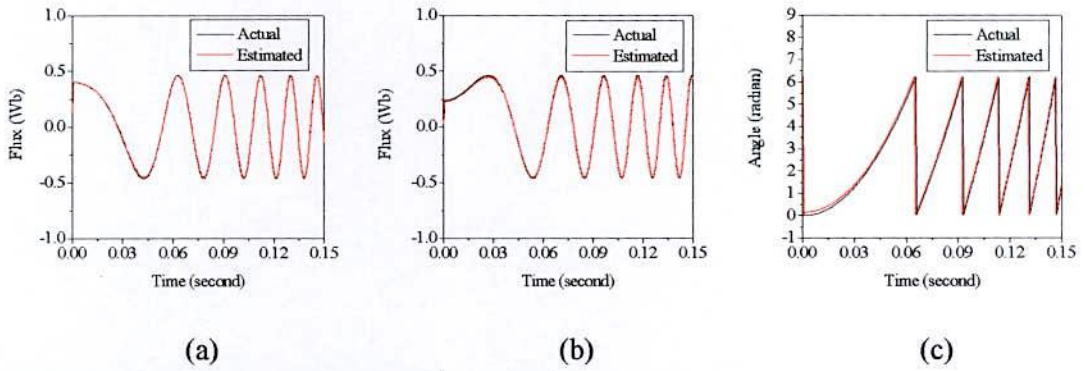


Figure 5.2.1 Actual and estimated responses of (a) α -axis stator flux, (b) β -axis stator flux, and (c) Rotor angle for the 6S3P inverter fed PMSM drive (runs at 1500 rpm) under transient condition.

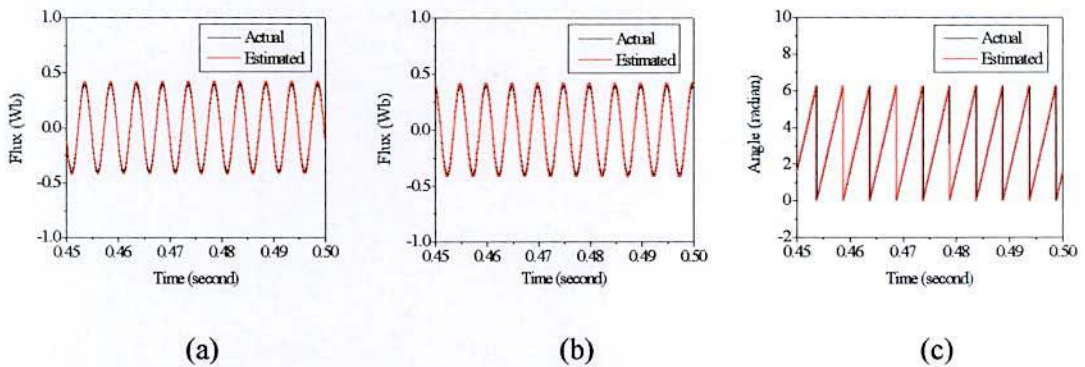


Figure 5.2.2 Actual and estimated responses of (a) α -axis stator flux, (b) β -axis stator flux, and (c) Rotor angle for the 6S3P inverter fed PMSM drive (runs at 1500 rpm) under steady-state condition.

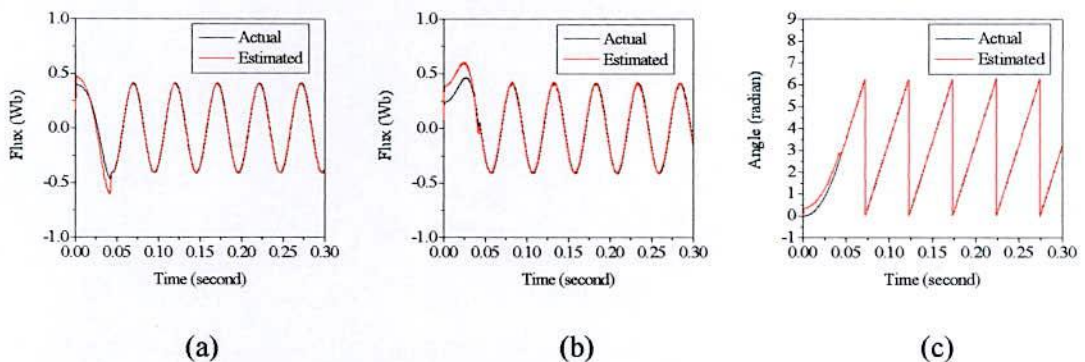


Figure 5.2.3 Actual and estimated responses of (a) α -axis stator flux, (b) β -axis stator flux, and (c) Rotor angle for the 6S3P inverter fed PMSM drive (runs at 150 rpm) under transient and steady-state conditions.

5.3 Starting Performance of the PMSM Drive

The motor was started with a command speed of 1500 rpm and load torque of 1.0 N.m from standstill condition. At $t=0.45$ second the motor reaches to the command speed. Fig. 5.3 and 5.4 show the stator voltages supplied to the motor by the 4S3P and 6S3P inverters, respectively. In case of 4S3P inverter the a -phase and b -phase voltages have almost similar characteristics but the c -phase voltage is different in nature. Therefore, the 3-phase voltages produced by the 4S3P inverter are in unbalanced condition. Whereas, the 6S3P inverter produces balanced 3-phase voltages for driving the motor.

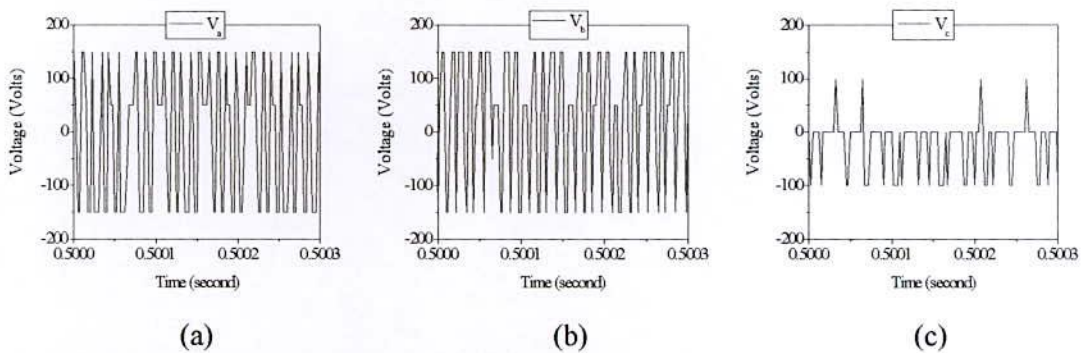


Figure 5.3 Stator phase voltages for the 4S3P inverter fed PMSM: (a) V_a , (b) V_b , (c) V_c .

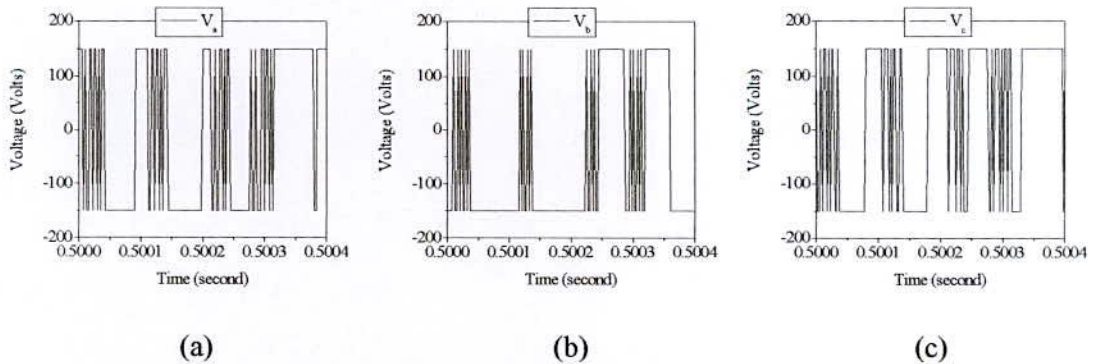


Figure 5.4 Stator phase voltages for the 6S3P inverter fed PMSM: (a) V_a , (b) V_b , (c) V_c .

Figs. 5.5 and 5.6 show the speed response, developed electromagnetic torque, command currents and actual motor currents for the PMSM drive with 4S3P and 6S3P inverter respectively. In both cases the actual speed follows the command speed accurately without steady-state error and oscillations. It is also observed that higher electromagnetic torque is

developed during the motor acceleration. Some oscillations in electromagnetic torque is noticed which is due to switching of the devices with hysteresis controller. Difference between developed and load torques is due to viscous damping torque of the drive system. The three phase command currents are obtained from vector rotator. The three phase actual moors currents are obtained using Park's reverse transformation. It is noticed that the motor follows the command currents efficiently. The currents obtained from 4S3P inverter fed drive seem to be slightly non-sinusoidal in nature. But this unbalanced characteristic of the 4S3P inverter does not hamper the speed response of the drive.

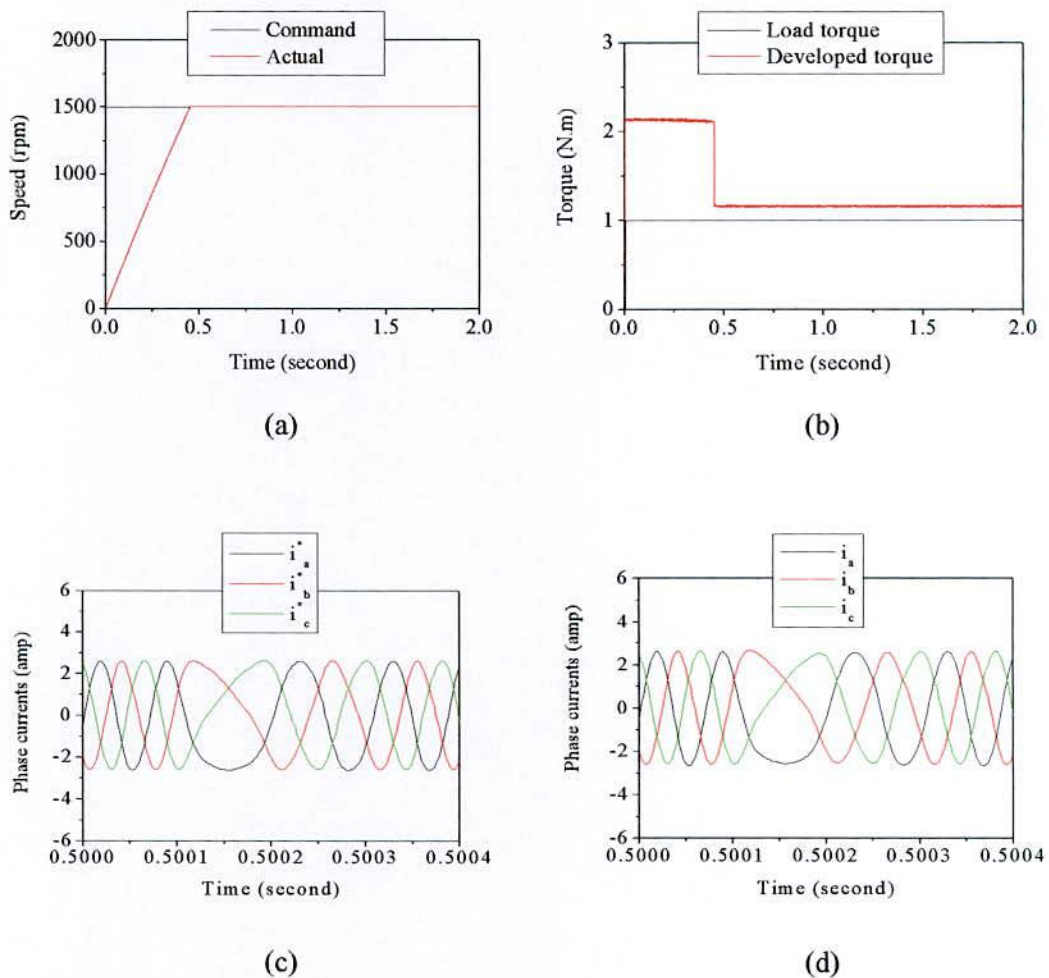
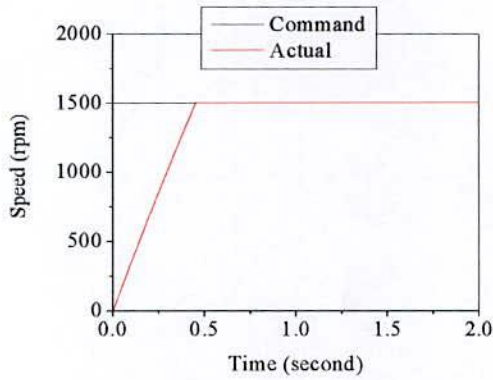
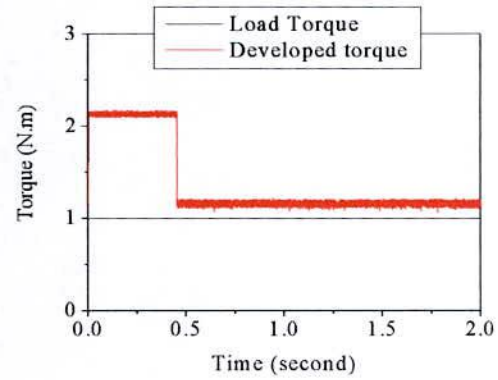


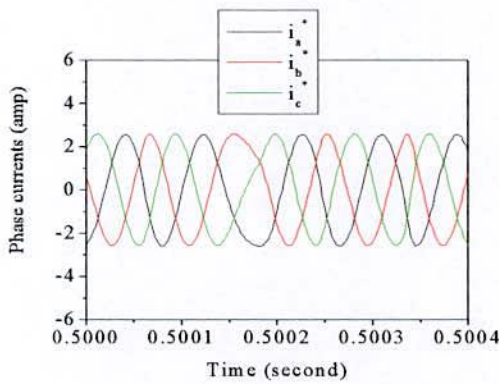
Figure 5.5 (a) Speed, (b) Developed electromagnetic torque, (c) command currents, and (d) actual motor currents for the 4S3P inverter fed PMSM drive.



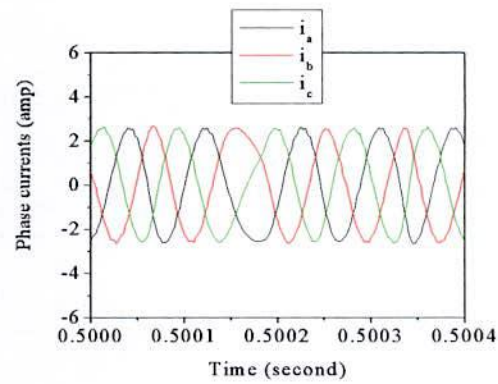
(a)



(b)



(c)



(d)

Figure 5.6 (a) Speed, (b) Developed electromagnetic torque, (c) command currents, and (d) actual motor currents for the 6S3P inverter fed PMSM drive.

5.4 Performance under Different Operating Conditions

The performance of the PMSM drive under different operating conditions was also investigated in order to verify the robustness of the proposed control scheme. The corresponding responses and their descriptions are given in the following sub-sections.

5.4.1 Sudden Change of Load Torque

Initially the motor was started from standstill with load torque 1 N.m. Suddenly at $t=1.0$ second the load torque was increased to 2.0 N.m. The estimated rotor angle and the speed responses for change of load torque are given in Figs. 5.7(a) and (b). Sudden change of

load torque does not affect the position estimation and causes a negligible oscillation in speed. Figs. 5.7(c) and (d) show the corresponding torque and motor currents. The motor currents increase after 1.0 second due to the increase of load torque.

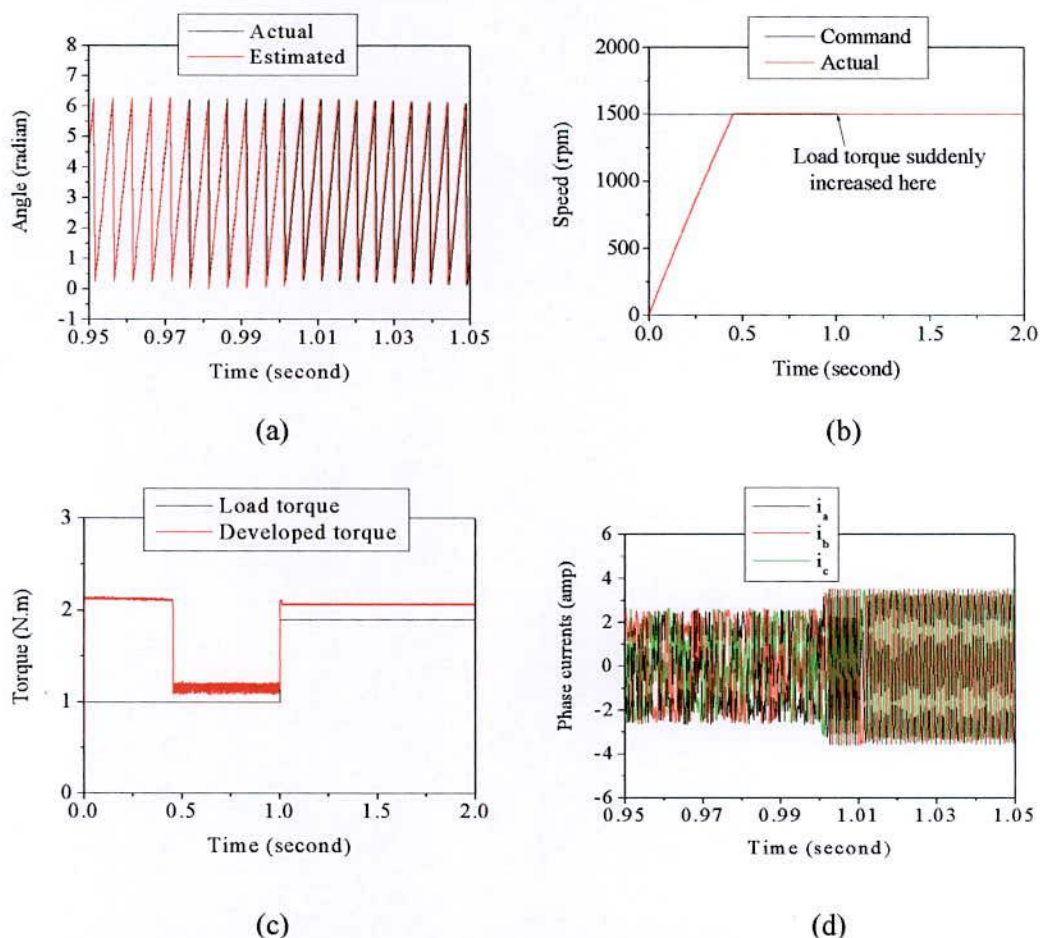


Figure 5.7 (a) Estimated rotor angle, (b) Speed, (c) Developed electromagnetic torque, and (d) Three phase currents for the proposed PMSM drive for change of load torque.

5.4.2 Variation of Stator Parameters

To observe the effect of parameter variations, the motor stator resistance was doubled (keeping other parameters constant) at $t = 1.0$ second. Fig. 5.8(a) shows the effect of stator resistance change on angle estimation. The estimated angle still follows the actual angle. Thus the change in resistance has negligible effect on the accuracy of rotor position estimation. Fig. 5.8(b) shows the effect of stator resistance change on speed response. The speed does not drop at all due to change of stator resistance. Thus the drive performance is

insensitive of stator parameter variation. Figs. 5.8(c) and (d) show that the developed torque and motor currents are also insensitive to stator parameter variation.

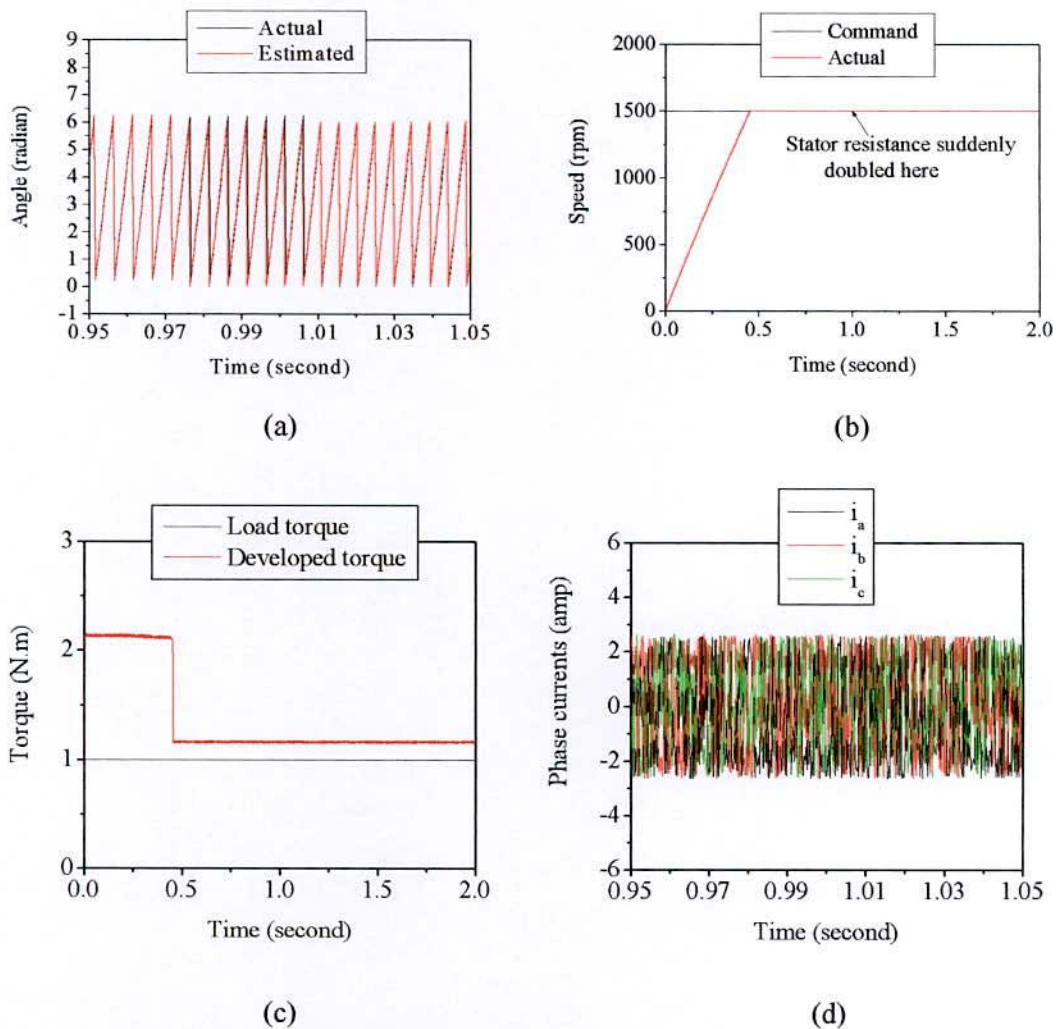


Figure 5.8 (a) Estimated rotor angle, (b) Speed, (c) Developed electromagnetic torque, and (d) Three phase currents for the proposed PMSM drive for change of stator resistance.

5.4.3 Speed Reversal

Speed reversal is an essential requirement for high performance PMSM drives. Therefore, to monitor the effect of speed reversal, the command speed of the motor was reversed from 1500 rpm to -1500 rpm at $t=0.6$ second and again to 1500 rpm at $t=1.4$ second. Fig. 5.9(a) shows estimated rotor angle when the motor runs at -1500 rpm. There is slight error between the estimated and actual angle but it is within the acceptable limit. The speed

response for different set speeds is shown in Fig. 5.9(b). It is observed that the drive system follows both the forward and reverse direction reference track very quickly. The impact on developed electromagnetic torque and motor current due to speed reversal is shown in Fig. 5.9(c) and (d). The proposed control scheme produces less torque fluctuation at steady-state condition.

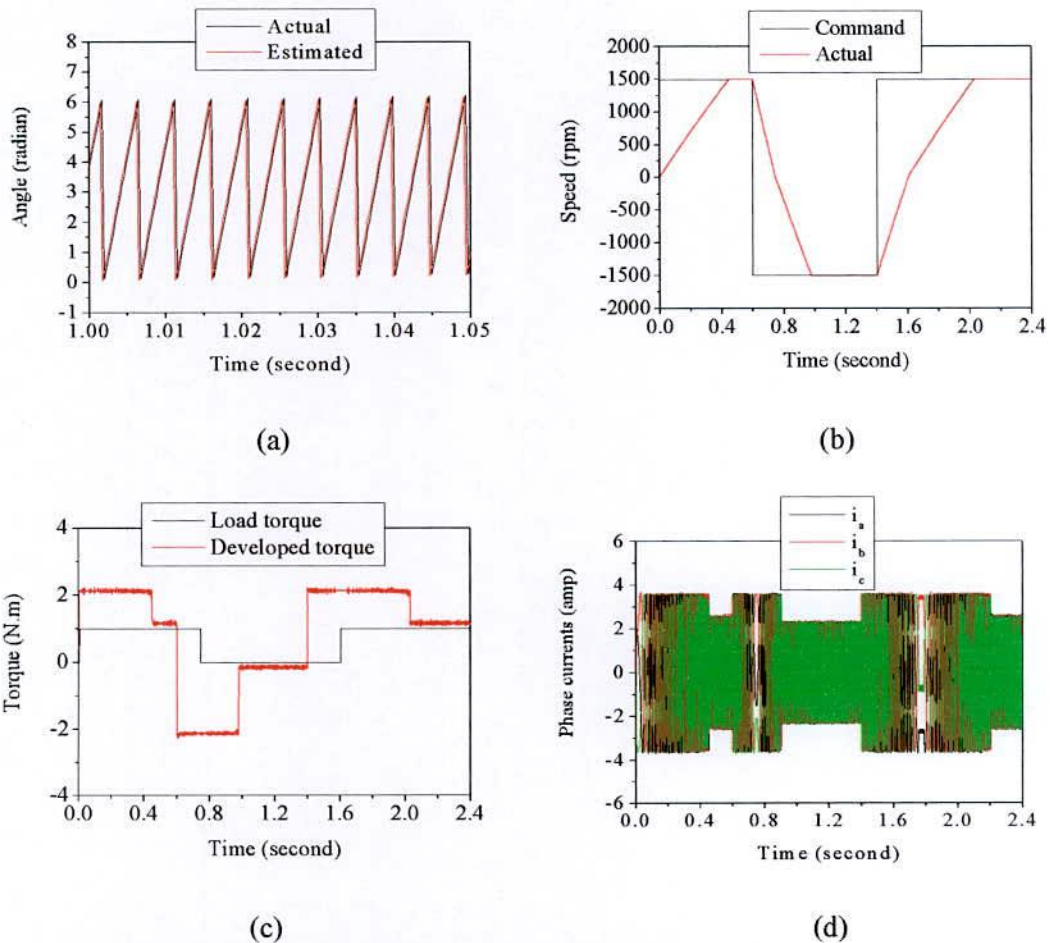


Figure 5.9 (a) Estimated rotor angle, (b) Speed, (c) Developed electromagnetic torque, and (d) Three phase currents for the proposed PMSM drive under speed reversal.

5.4.4 Ramp Speed Change

Like as speed reversal, ramp speed is also an essential requirement for high performance PMSM drives. The controller set speed was gradually increased from zero and at time $t=1.0$ second it remained constant to 1500 rpm value. The estimated rotor position, speed

response, developed electromagnetic torque and motor currents are shown in Fig. 5.10. The motor follows the command speed from the starting without any oscillation and steady-state error. The developed torque response is also similar to the starting performance.

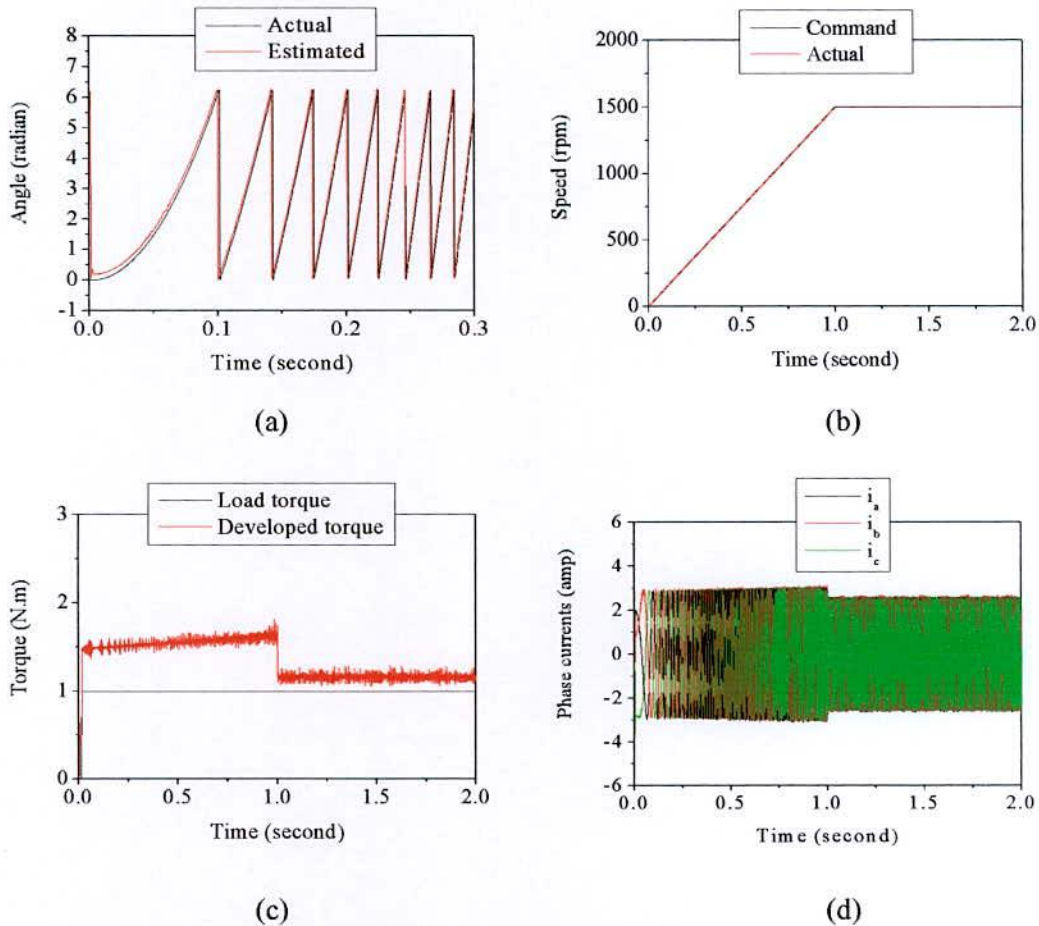


Figure 5.10 (a) Estimated rotor angle, (b) Speed, (c) Developed electromagnetic torque, and (d) Three phase currents for the proposed PMSM drive under ramp speed change.

5.4.5 Sudden Disturbance Torque

A sudden load torque disturbance (1.5 N.m) for a very short duration of 0.1 second was applied to the PMSM drive at time $t=1.0$ second. Fig. 5.11(a) shows the actual and estimated rotor angle of the motor at that time period. The speed response of the PMSM is shown in Fig. 5.11(b). Simulation studies show that the proposed control scheme is still capable to estimate the rotor angle accurately. Besides, the motor speed is insensitive to the

sudden torque disturbance. Fig. 5.11(c) and (d) show the corresponding developed torque and motor currents.

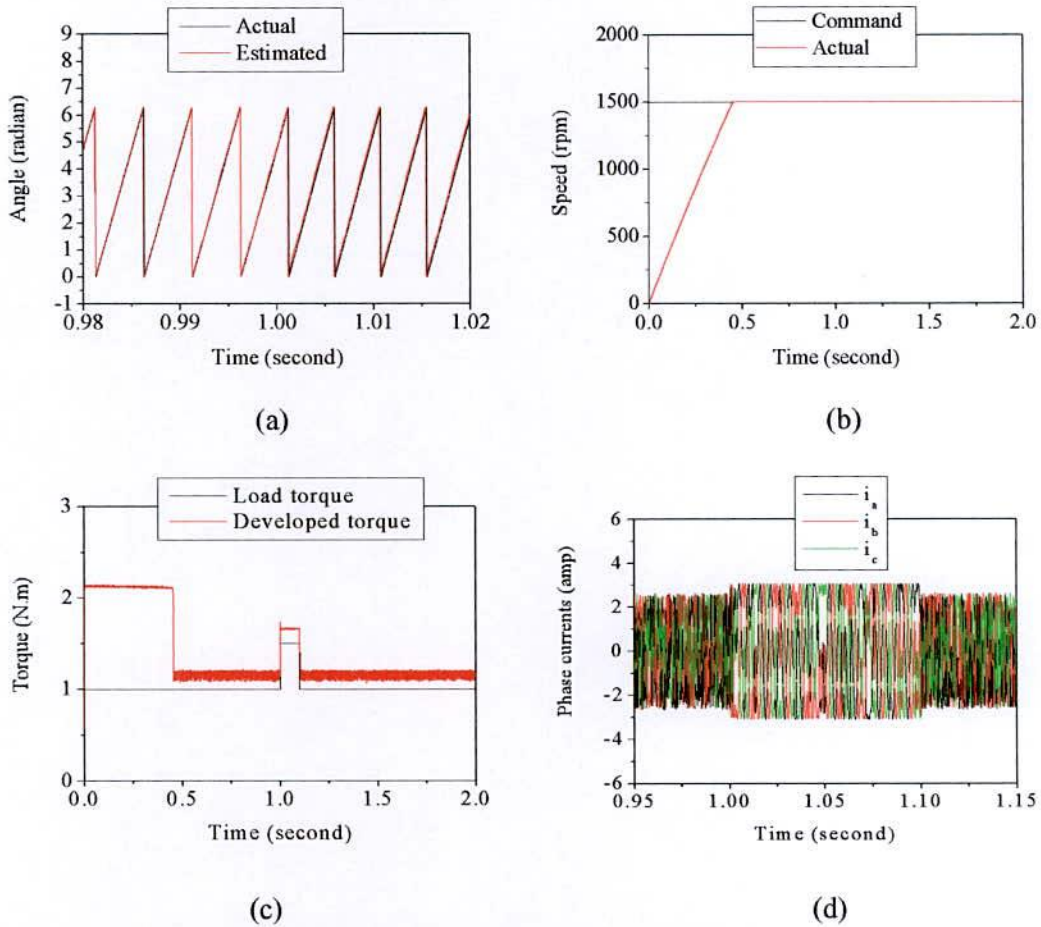
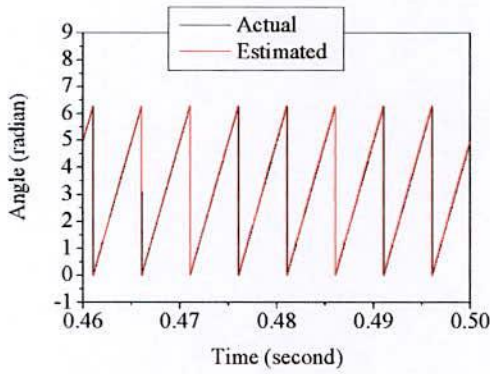


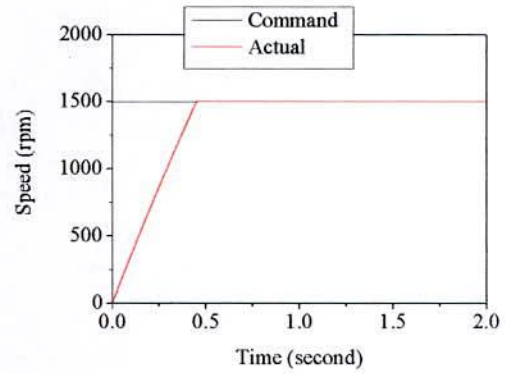
Figure 5.11 (a) Estimated rotor angle, (b) Speed, (c) Developed electromagnetic torque, and (d) Three phase currents for the proposed PMSM drive for sudden disturbance torque.

5.4.6 Presence of Computational Errors

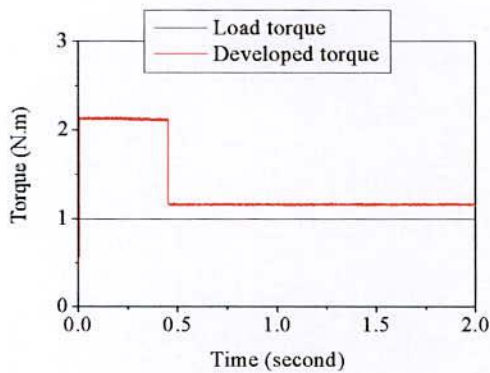
There is always some instrumental error present in physical system. For the robustness test $\pm 8\%$ instrumental error was introduced to the inverter dc voltage. The estimated and actual rotor angle of the PMSM is shown in Fig. 5.12(a). It is observed that the presence of computational error does not affect the estimation. The performance of motor speed, developed torque, and stator currents are presented in Fig. 5.12(b) to Fig. 5.12(d). Depending on the performances it can be claimed that the performance of the proposed control scheme is insensitive to the computational error within the range of -8% to 8%.



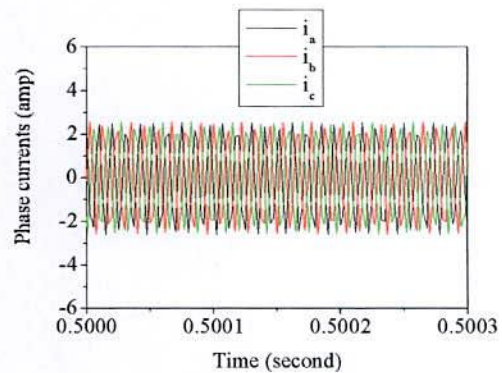
(a)



(b)



(c)



(d)

Figure 5.12 (a) Estimated rotor angle, (b) Speed, (c) Developed electromagnetic torque, and (d) Three phase currents for the proposed PMSM drive for computational error.

5.5 Conclusion

A detailed simulation model for the PMSM drive system has been developed and analyzed to investigate the performance of the proposed control scheme. A comparison of 4S3P inverter fed drive and 6S3P inverter fed drive is given. It is found that the 4S3P inverter fed drive provides almost similar speed, torque, and current responses as that of 6S3P inverter fed drive. The proposed RNN stator flux and rotor angle estimator is found to work accurately. The hysteresis current controller allows faster simulations with reduced time and computational resources. A speed controller has been designed successfully for the PMSM drive system so that the motor runs at the command speed. The proposed drive is also sufficiently stable and robust to load disturbances, perturbation of parameters, computational error and several other effects.

CHAPTER VI

Conclusions and Suggestions for Future Works

6.1 Conclusions

This dissertation covers two major issues and solutions dealing with cost-effective position sensorless control of permanent magnet synchronous motors over wide speed range. It accommodates the robust insensitive features of ANN estimator and advantages of 4S3P inverter. The 4S3P control system reduces the cost of the three phase inverter, the switching losses, and the complexity of the control algorithms. A detailed simulation Turbo C++ model for the PMSM drive system is developed and operation under different operating conditions is studied. The simulation results demonstrate the acceptability of the proposed control methodology for high performance application.

The first goal of this research was to find an optimal method to estimate the rotor position of the PMSM. Stable operation over wide speed range was also required. Therefore, recurrent neural network based stator flux and rotor position estimator is utilized. The weights of the neural network are obtained by training the network using correlated real time recurrent learning algorithm. The proposed estimator estimates α - and β - axis stator fluxes and found to work satisfactorily under transient and steady-state conditions. The estimated stator flux components are then used to estimate the position of the rotor and provide accurate results under both transient and steady-state conditions. The RNN estimator is capable to estimate the stator fluxes and rotor angle at low motor speed. The estimator is also accurate and robust to perturbation of parameters.

The vector control scheme is incorporated in the drive system to achieve high performance at different operating conditions. A PI speed controller is designed successfully for close loop operation of the PMSM drive system so that the motor runs at the command or reference speed. The switching logics of the 4S3P inverter are such that three voltages supplied to the motor are unbalanced. For this reason, in this study the voltages fed by the 4S3P inverter are found unequal. But it does not affect the speed response of the motor. The starting performance of the PMSM shows that the proposed control scheme produces

very fast response of the PMSM drive. The motor reaches to the command speed at 0.45 second and follow it without any steady-state error. The starting developed torque is almost twice the steady-state torque. The three phase stator currents are almost sinusoidal.

The performance of the PMSM drive is also investigated for different operating conditions. The proposed control scheme provides good speed response of the motor when the load torque fluctuates from its initial value. The PMSM drive follows the reference track very quickly during speed reversal and ramp change of speed. The system is also found robust against computational errors present in the physical system.

Based on the results from previous chapters and the above discussion it can be conclude that the proposed CRTRL based 4S3P control scheme is suitable for present industry applications.

6.2 Suggestions for Future Works

The research work presented in this dissertation provides a methodology to utilize the ANN for position sensorless operation of PMSM drive. The proposed system may be implemented in practical environment and compares the practical results with those obtained from this study. It is suggested that this work can also be tested for a Reluctance Synchronous Machine (RSM) with distributed stator winding, and a Permanent Magnet Assisted Reluctance Synchronous Machine (PMARSM) in order to verify the effectiveness of the proposed control methodology.

Selection of proper controller parameters is a challenge for the researchers in high performance drives. To produce required variable dynamics from the drive system PI controller constants may be obtained using online tuning through genetic or evolutionary algorithms. Further, the researchers may work with fuzzy-neuro estimators instead of RNN estimators. Newly introduced training methods, such as particle swarm optimization or bacterial foraging technique may be tested for training the estimators. These flux and position estimators are expected to work effectively under all operating conditions.

REFERENCES

- [1] Muhammad H. Rashid, 2004, "Power Electronics Circuits, Devices, and Applications", Chapter 16, pp. 692, Pearson Education, 3rd Edition.
- [2] Junggi Lee, Jinseok Hong, Kwanghee Nam, Romeo Ortega, Laurent Praly, and Alessandro Astolfi, 2010, "Sensorless Control of Surface-Mount Permanent-Magnet Synchronous Motors Based on a Nonlinear Observer," IEEE Transactions on Power Electronics, Vol. 25, No. 2, pp. 290-297.
- [3] A. B. Dehkordi, A. M. Gole, and T. L. Maguire, 2005, "Permanent Magnet Synchronous Machine Model for Real-Time Simulation," Proceedings of International Conference on Power Systems Transients, Montreal, Canada.
- [4] Weera Kaewjinda and Mongkol Konghirun, 2007, "Vector Control Drive of Permanent Magnet Synchronous Motor Using Resolver Sensor," ECTI Transactions on Electrical Eng., Electronics, and Communications, Vol. 5, No. 1, pp. 134-138.
- [5] B. K. Bose, 1993, "Power electronics and motion control-Technology status and recent trends," IEEE Trans. on Industry Applications, Vol. 29, pp. 902-909.
- [6] W. Leonhard, 1988, "Adjustable speed ac drives," Proceedings of IEEE, Vol. 76, pp. 455-471.
- [7] B. K. Bose, 1993, "Variable frequency drives-technology and applications," Proceedings of ISIE 93, pp 1-18, Budapest.
- [8] S.Saravanasundaram and K.Thanushkodi, 2008, "Compound Active Clamping Boost Converter-Three Phase Four Switch Inverter Fed Induction Motor," International Journal of Computer Science and Network Security, Vol. 8, No. 8, pp. 358-361.
- [9] M. N. Uddin, T. S. Radwan, and M. A. Rahman, 2006, "Performance Analysis of a Cost Effective 4-Switch, 3-Phase Inverter Fed IM Drive," Iranian Journal of Electrical and Computer Engineering, Vol. 5, No. 2, pp. 97-102.
- [10] M. N. Uddin, T. S. Radwan, and M. A. Rahman, 2004, "A Cost Effective 4-Switch, 3-Phase Inverter Fed PM Motor Drive," Proceedings of International Conference on Electrical & Computer Engineering, pp. 339-342, Dhaka, Bangladesh.
- [11] M. N. Uddin, T. S. Radwan, and M. A. Rahman, 2006, "Fuzzy-logic-controller-based cost effective four-switch three-phase inverter-fed IPM synchronous motor drive system," IEEE Trans. on Industry Applications, Vol. 42, No. 1, pp. 21-30.

- [12] Phan Quoc Dzung, Le Minh Phuong, Tran Cong Binh, and Nguyen Minh Hoang, 2007, "A Complete Implementation of Vector Control for a Four-Switch Three-Phase Inverter Fed IM Drive," International Symposium on Electrical & Electronics Engineering, HCM City, Vietnam.
- [13] Koji Tanaka and Ichiro Miki, 2007, "Position Sensorless Control of Interior Permanent Magnet Synchronous Motor Using Extended Electromotive Force," Electrical Engineering in Japan, Vol. 161, No. 3, pp. 41-48.
- [14] Xu Z., Rahman M. F., 2004, "Encoder-Less Operation of a Direct Torque Controlled IPM Motor Drive with a Novel Sliding Mode Observer," Proceedings of AUPEC 2004, Australia.
- [15] Satoshi Ogasawara and Hirofumi Akagi, 1998, "Implementation and Position Control Performance of a Position-Sensorless IPM Motor Drive System based on Magnetic Saliency," IEEE Trans. on Industry applications, Vol. 34, No. 4, pp. 806-812.
- [16] Ion Boldea, Ana Moldovan, Vasile Coroban Schramel, Gheorghe Daniel Andreescu, and Lucian Tutelea, 2010, "A Class of Fast Dynamics V/f Sensorless AC General Drives with PM-RSM as a Case Study," Proceedings of OPTIM 2010, Romania.
- [17] Hugo W. De Kock, Maarten J. Kamper, and Ralph M. Kennel, 2009, "Anisotropy Comparison of Reluctance and PM Synchronous Machines for Position Sensorless Control Using HF Carrier Injection," IEEE Transactions on Power Electronics, Vol. 24, No. 8, pp. 1905-1913.
- [18] Joao O.P. Pinto, Bimal K. Bose, and Luiz Eduardo Borges da Silva, 2001, "A Stator-Flux-Oriented Vector-Controlled Induction Motor Drive with Space Vector PWM and Flux-Vector Synthesis by Neural Networks," IEEE Trans. on Industry applications, Vol. 37, No. 5, pp. 1308-1318.
- [19] Sung-Hoe Huh, Kyo-Beum Lee, Dong-Won Kim, Ick Choy, and Gwi-Tae Park, 2005, "Sensorless Speed Control System Using a Neural Network," International Journal of Control, Automation, and Systems, Vol. 3, No. 4, pp. 612-619.
- [20] Sencer Unal, Mehmet Ozdemir, 2007, "Sensorless Control of the Permanent Magnet Synchronous Motor Using Neural Networks," Proceedings of ACEMP 2007, Turkey.
- [21] Manoj Datta, Md. Abdur Rafiq, Mohammed Golam Sarwer, and B. C. Ghosh, 2005, "An Efficient Induction Motor Rotor Flux Estimator Based on Real Time Recurrent Learning Algorithm," Proceedings of the International Conference on Intelligent Systems, Malaysia.

- [33] B. Widrow and S. D. Stearn, 1985, "Adaptive Signal Processing," Englewood Cliffs, NJ: Prentice-Hall.
- [34] B. K. Bose and N. R. Patel, 1997, "A Sensorless Stator Flux Oriented Vector Controlled Induction Motor Drive with Neuro-Fuzzy Based Performance Enhancement," Proceedings of the IEEE IAS'97 (Ind. Application Soc. Annual Meeting), Oct. 5-9.
- [35] S. Bologani, G. S. Buja, 1985, "Control System Design of a Current Inverter Induction Motor Drives," IEEE Trans. on Industry Applications, Vol. IA-21, No. 5, pp. 1145-1153.

APPENDIX

PMSM Parameters and Nameplate Data/Rating:

Rating:

3-phase, 1 hp, 208V, 3A, 2-pole pair.

Parameters:

Table A1: PMSM Parameters

Sl. No.	Parameters	Values in SI units
1	Stator resistance, r_s	1.3 Ω
2	d -axis inductance, L_d	0.04244 H
3	q -axis inductance, L_q	0.07957 H
4	Motor inertia, J_m	0.003 Kg-m ²
5	Friction coefficient, B_m	0.001 N-m/rad/s
6	Magnetic flux constant, ψ_f	0.311 Volts/rad/s

Weights of the RNN:

$W_{11} = W_{22} = 0.1$, $W_{12} = W_{21} = 0.0001$, $W_{13} = W_{24} = 0.068$, $W_{14} = -W_{23} = 0.05$, $W_{15} = W_{25} = 0.0001$.